ACS OMEGA

http://pubs.acs.org/journal/acsodf

Article

Delineating the Mechanism of Action of a Protease Resistant and Salt Tolerant Synthetic Antimicrobial Peptide against *Pseudomonas aeruginosa*

Gopal Pandit, Tanumoy Sarkar, Vignesh S. R., Swapna Debnath, Priyadarshi Satpati,* and Sunanda Chatterjee*

Cite This: *ACS Omega* 2022, 7, 15951−15968

Read Online

ACCESS | Metrics & More | Article Recommendations | Supporting Information

ABSTRACT: Rapidly growing antimicrobial resistance (AMR) against antibiotics has propelled the development of synthetic antimicrobial peptides (AMPs) as potential antimicrobial agents. An antimicrobial peptide Nle-Dab-Trp-Nle-Dab-Dab-Nle-$CONH_2$ (**P36**; Nle = norleucine, Dab = diaminobutyric acid, Trp = tryptophan) potent against *Pseudomonas aeruginosa* (*P. aeruginosa*) has been developed in the present study. Rational design strategy adopted in this study led to the improvisation of the therapeutic qualities such as activity, salt tolerance, cytotoxicity, and protease resistance of the template peptide **P4**, which was earlier reported from our group. **P36** exhibited salt tolerant antimicrobial potency against *P. aeruginosa*, along with very low cytotoxicity against mammalian cell lines. **P36** was found to be nonhemolytic and resistant toward protease degradation which qualified it as a potent antimicrobial agent. We have investigated the mechanism of action of this molecule in detail using several experimental techniques (spectroscopic, biophysical, and microscopic) and molecular dynamics simulations. **P36** was a membrane active AMP with membrane destabilization and deformation abilities, leading to leakage of the intracellular materials and causing eventual cell death. The interaction between **P36** and the microbial membrane/membrane mimics was primarily driven by electrostatics. **P36** was unstructured in water and upon binding to the microbial membrane mimic SDS, suggesting no influence of secondary structure on its antimicrobial potency. Positive charge, optimum hydrophobic−hydrophilic balance, and chain length remained the most important concerns to be addressed while designing small cationic antimicrobial peptides.

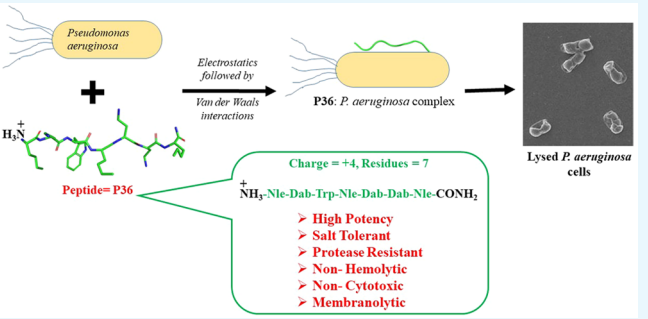

1. INTRODUCTION

Growing antimicrobial resistance (AMR) leading to development of multidrug resistant (MDR) microbes[1] imposes a great threat to human civilization.[2,3] The problem is augmented by the slowdown in the development of new classes of antibiotics.[4] Thus, there is an urgent need for development of alternate classes of therapeutic molecules to combat microbial infections. Antimicrobial peptides (AMPs) are a class of small proteins, which have antimicrobial activity and are present in various kingdoms of life. They act as the first line of the innate defense system of the host against several microbes such as bacteria, fungi, yeasts, viruses, and parasites.[5] These peptides have diverse sequences and secondary structures. The major advantage of the AMPs over the conventional antibiotics lies in the fact that they develop resistance in microbes much more slowly in comparison to the latter.[6] Multiple modes of action of the AMPs, such as membrane disruption, membrane permeabilization leading to severance of intracellular mechanisms and pathways,[7−9] and immunomodulatory activities, in contrast to the specific targets of the antibiotics, are responsible for the delayed development of resistance against them in the microbes. Additionally, being constituted of the biocompatible materials, AMPs generate nontoxic metabolites in comparison to the antibiotics. A large class of AMPs are cationic in nature. Electrostatic interaction between the positively charged peptides and the negatively charged membrane surfaces of the microbes lead to membrane binding, depolarization, deformation, membrane leakage, and eventual cell death.[10,11]

The Gram-negative bacterial infections are more difficult to treat than the Gram-positive bacterial infections.[2,4,12] This is owing to the lipopolysaccharide (LPS) layer which forms the outer leaflet of the asymmetrical lipid bilayer in the Gram-negative bacteria.[13,14] The AMP encounters the LPS layer in

Received: February 23, 2022
Accepted: April 8, 2022
Published: April 29, 2022

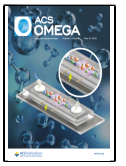

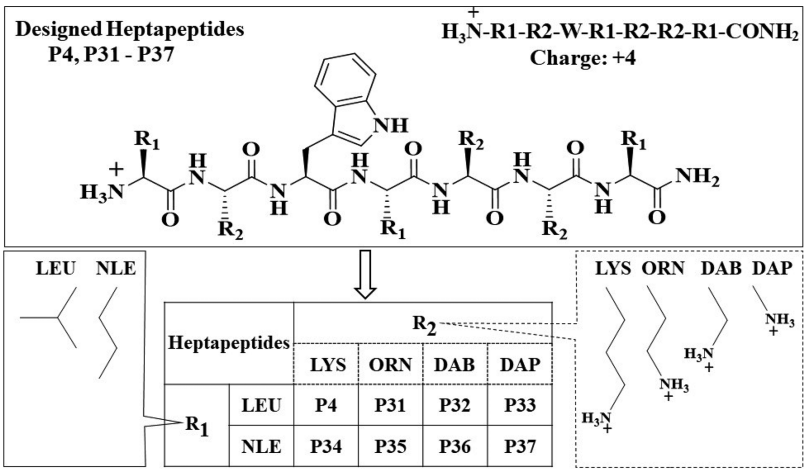

Figure 1. Schematic representation of the heptapeptides (**P31**−**P37**) designed from the all α amino acid containing template peptide **P4**. In peptides **P31**−**P33**, polar amino acid Lys of **P4** was replaced by unnatural analogs such as Orn, Dab, and Dap; in **P34**, all of the nonpolar hydrophobic Leu residues in **P4** were replaced by Nle; and in **P35**−**37**, both the Lys and Leu residues were simultaneously replaced by the unnatural analogs. The side chains of the unnatural amino acid residues are illustrated in the figure.

the Gram-negative bacteria before it can assess the inner plasma membrane.[15,16] The LPS layer interacts with the antibiotics and the AMPs, rendering them inactive. The resistance of the Gram-negative bacteria against the AMPs is partially attributed to the LPS layer, though there are other known mechanisms of the development of resistance against them such as chemical modification of the lipid membranes, sequestration, proteolytic degradation, release of glycosaminoglycans (GAGs), polysaccharides, and polyanionic scavenging species.[17−19]

In spite of such huge potential of the AMPs, only a few of them, such as Bacitracin, Daptomycin, Vancomycin, Boceprevir, Telaprevir, etc., are commercially used as antimicrobial therapeutics.[20] This is largely owing to the disadvantages that are associated with natural AMPs such as large sequences leading to high cost of synthesis, low serum stability owing to the protease degradation, salt sensitivity of antimicrobial potency,[21−24] and toxicity to mammalian cells.[25] Cationic antimicrobial peptides have large quantities of lysine (Lys) and arginine (Arg), making them highly susceptible to serine proteases such as trypsin, which specifically hydrolyzes the peptide bond at the C-terminal end of the Lys and Arg. In an effort to overcome the protease degradability of the AMPs, different strategies have been adopted such as (a) insertion of nonstandard ω-amino acids[26−28] and side-chain-modified α-amino acids[29−31] in the AMP sequence, (b) peptide terminal modifications,[29−31] (c) insertion of amino acids of opposite chirality,[32−34] (d) cyclization of the AMP sequences,[35−37] (e) insertion of peptidomimetic blocks in key positions of the sequence,[38−42] (f) pegylation,[43−45] (g) lipidation,[46,47] and (h) construction of hybrids.[48] Of all the strategies employed, modification of the side-chain length of the positively charged amino acid residues, such as Lys and Arg, is the most common one. Many nonstandard amino acids are used as analogs of Lys, such as Ornithine (Orn), Dab (diaminobutyric acid), Dap (diaminopropionic acid), and Arg such as homoarginine 2-amino(3-guanidino)propanoic acid.[49−57] In general, the short-side-chain analogs for Lys and the long-side-chain analogs for Arg, improved the activity of the AMPs.

In an earlier study from our group, we had reported a cationic heptapeptide, P4 ($LKWLKKLCONH_2$), with broad spectrum activity against ESKAPE pathogens and fungal strains in vitro.[58] Due to the all α-amino acid backbone and high content of Lys, **P4** can be anticipated to be susceptible to protease degradation in vivo. In the present study, we wanted to impart protease resistance to **P4** by replacing the α-amino acids by their nonstandard analogous amino acids. The designed analogs of **P4** (**P31**−**P37**, Figure 1) had identical charge but differed in their hydrophobic−hydrophilic balance. Because the hydrophobic−hydrophilic balance plays a crucial role in determining the bioactivities of the AMPs, we investigated the antimicrobial potency, salt tolerance, and cytotoxicity of the designed peptides **P31**−**P37**. The mechanism of action of the lead AMP was studied in detail using various biophysical, spectroscopic, microscopic techniques, as well as computational analysis.

2. RESULTS AND DISCUSSION

2.1. Rational Design of the AMPs. Peptides **P31**−**P37** were designed on the basis of **P4**, an earlier reported peptide,[58] as a template (Figure 1; Supporting Information Tables S3 and S4). In an attempt to improve the activity and protease resistance of **P4**, Lys and Leu in the sequence were systematically mutated by side-chain-modified analogs of Lys (Orn, Dab, Dap) and Leu (Nle). Mutations were systematically incorporated to change the polar (**P31**−**P33**) and hydrophobic (**P34**) amino acid residues, one type at a time or both simultaneously (**P35**−**P37**). The side-chain length and the hydrophobicity of Lys and its analogs diminish in the order of Lys, Orn, Dab, and Dap. Though the side-chain carbon atoms are the same for Nle and Leu, the former is longer, being unbranched in comparison to the later, which is branched. Thus, though all of the **P4** analogs (**P31**−**P37**) studied here had charge identical to that of **P4**, their overall hydrophobicities were different due to incorporation of various nonstandard amino acid analogs of Lys and Leu.

2.2. Peptide Synthesis and characterization. All of the designed peptides were synthesized using a solid-phase synthesis protocol as described in the Experimental Section. The purified peptides were characterized using analytical HPLC (Figures S2−S8), ESI-MS (Figures S9−S15), and ^{1}H NMR (Figures S16−S22) spectra.

https://doi.org/10.1021/acsomega.2c01089
ACS Omega 2022, 7, 15951−15968

Table 1. $MIC_{99\%}$ of P31−P37 against ESKAPE pathogens *P. aeruginosa*, *K. pneumoniae*, and *S. aureus*[a]

microbe	$MIC_{99\%}$ (μM)					
	Gram negative bacteria				Gram positive bacteria	
	P. aeruginosa		*K. pneumoniae*		*S. aureus*	
peptide	absence of salts	presence of salts	absence of salts	presence of salts	absence of salts	presence of salts
P4 (control)	30	ND*	50	ND*	80	ND*
P31	20	ND*	200	ND*	60	ND*
P32	20	100	60	ND*	40	ND*
P33	200	ND*	>200	ND*	200	ND*
P34	60	ND	200	ND	200	ND
P35	60	ND	200	ND	200	ND
P36	20	50	80	ND	20	ND
P37	60	ND	>200	ND	200	ND

[a]All of the $MIC_{99\%}$ are reported in μM. ND = not detectable; ND* = not done.

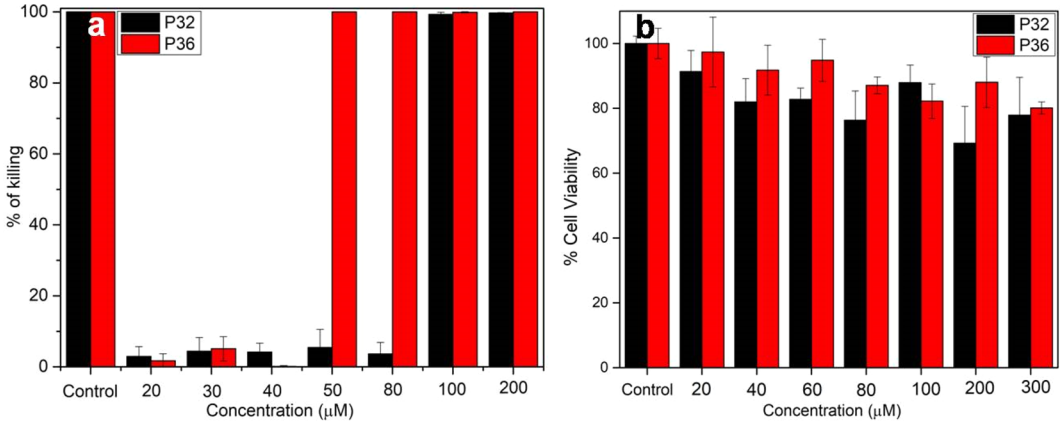

Figure 2. (a) Salt tolerant activity of **P32** (black) and **P36** (red) against *P. aeruginosa*. $MIC_{99\%}$ was calculated from the microbroth dilution assay performed in the presence of 150 mM NaCl. The control experiment was performed in the presence of 10 μM Polymixin B, and other readings were normalized against it. (b) MTT assay of the peptides **P32** (red) and **P36** (black) on L132 cell lines. Cell viability was measured by monitoring the absorbance at 570 nm upon addition of increasing concentrations of peptide to the cells. All of the experiments were performed in triplicate.

2.3. Antimicrobial activity of the designed AMPs. Antimicrobial activities of **P31−P37** were tested against both Gram-negative (*Pseudomonas aeroginosa* (*P. aeruginosa*) and *Klebsiella pneumoniae* (*K. pneumoniae*) and Gram-positive (*Staphylococcus aureus* (*S. aureus*)) ESKAPE pathogens. The activities of all of the peptides were compared with those of **P4** (Table 1; Figure S23). Activities of the peptides were dependent both on the individual sequences and on the bacterial strain. Activity against *P. aeruginosa* improved upon substitution of Lys with shorter side chains containing amino acids such as Orn and Dab in **P31** and **P32**/**P36** respectively. Upon further shortening of the side length of Lys by substituting it with Dap, the activity of **P33** diminished against *P. aeruginosa*. However, upon introducing the second type of substitution of Leu with Nle in **P37**, in addition to substitution of Lys with Dap, the activity against *P. aeruginosa* was partially recovered. In the case of **P35** and **P36** though, substitution of Leu with Nle did not improvise the activities of **P31** and **P32**, respectively. None of the analogs of **P4** showed enhanced activity compared to **P4** against *K. pneumoniae*. However, among the various analogs. those containing Dab (**P32**/**P36**) mutated in the place of Lys showed the best activity. In the case of Gram-positive bacteria *S. aureus*, **P32** containing Dab residues had improved activity in comparison to **P4**. The activity of **P32** further improved upon additional mutation of the Leu residues to Nle in **P36**. Activities of **P31** containing Lys to Orn substitution was somewhat comparable to that of **P4**, while the activity was lost upon introducing the double mutation involving both Lys and Leu residues in **P35**. Peptides **P33** and **P37** containing Dap mutations were completely inactive against *S. aureus*. **P34**, with Leu to Nle mutations, had somewhat diminished activity against *P. aeruginosa* and completely lost activity against *K. pneumoniae* and *S. aureus* in comparison to **P4**. This differential behavior of the designed AMPs against a specific microbes suggested that the hydrophobic−hydrophilic balance of the AMPs and the length of the side chains of the constituent amino acid residues were very important for their activities. Among the similarly charged cationic AMPs, this might be the factor that modulates activity. Secondly, the differential potency of a particular AMP toward the various microbial strains suggested that the activity depended on the membrane diversity of these strains.

Because most of the AMPs lose their activity in the presence of the physiological concentration of salt,[59] we investigated the salt tolerance of the antimicrobial activity of **P31−P37** in the presence of physiological concentrations of NaCl (150 mM), the most abundant salt in the serum. The loss of activity in the presence of salts is generally attributed to the electrostatic reasons that decrease the affinity of the cationic AMPs toward the negatively charged microbial membranes. The presence of salt delays the kinetics of the interaction between the peptide and the membrane surface though, the interaction network in

https://doi.org/10.1021/acsomega.2c01089
ACS Omega 2022, 7, 15951−15968

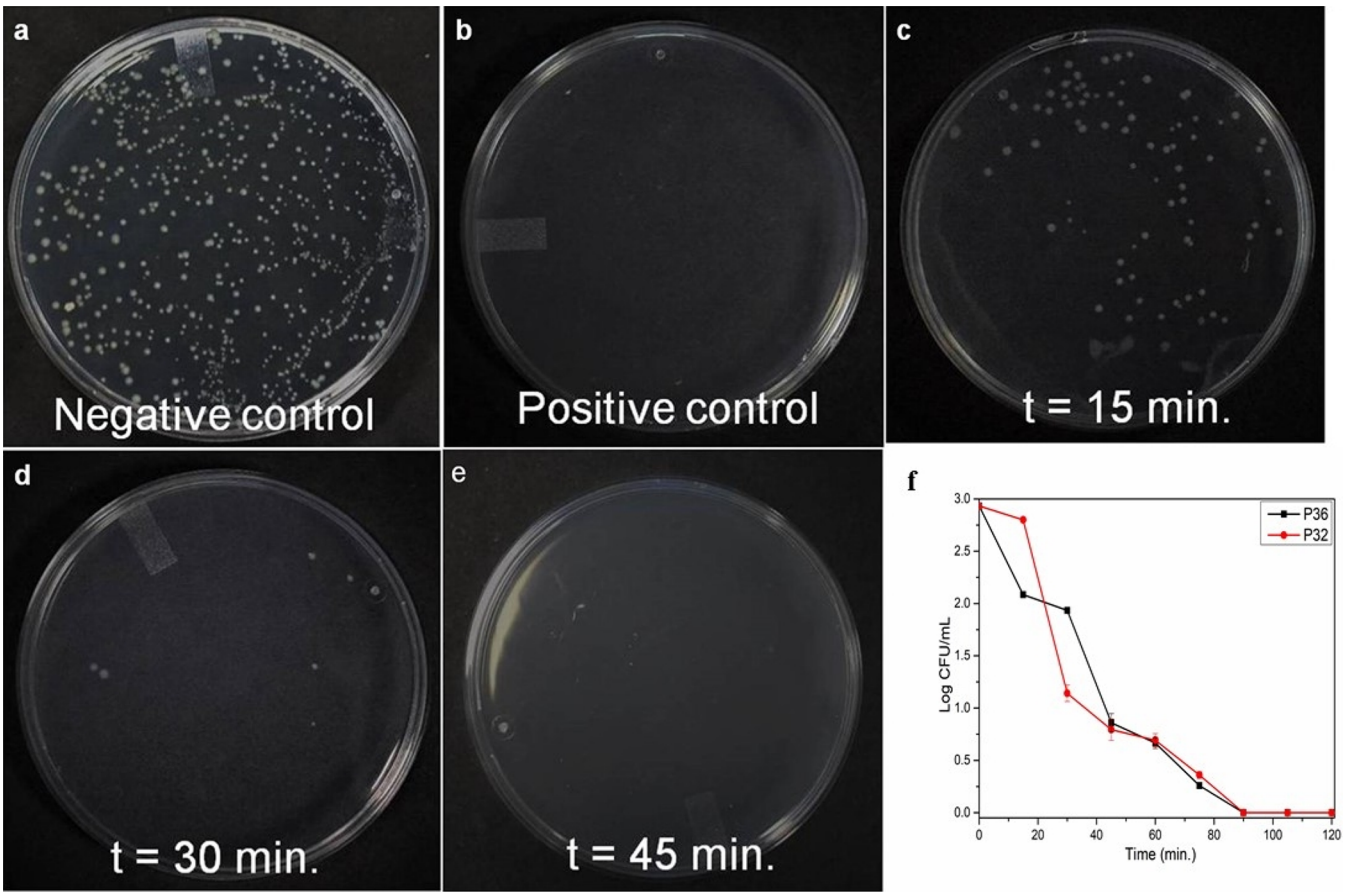

Figure 3. Time kinetics of the bactericidal activity of **P36** at its $MIC_{99\%}$ against *P. aeruginosa* cells. *P. aeruginosa* cells were treated with **P36** at MIC for different time intervals, and cells were spread on NA plate for CFU count after overnight incubation at 37 °C. Bacterial killing percentage was calculated from CFU count of the plate in comparison to the control plate. At 45 min time point, a completely clear plate was observed, suggesting a 100% killing of the microbial cells. (a) Negative control plate (no **P36** added), (b) positive control plate (10 μM Polymyxin B treated cells), and (c–e) plates at time points 15, 30, and 45 min, respectively. (f) Time kill kinetics of **P32** and **P36** against *P. aeruginosa*, shown in log scale.

the final peptide: membrane-mimetic complex is salt independent .[60] Of all the peptides designed, **P36** exhibited moderate NaCl tolerant activity respectively against *P. aeruginosa* (Figure 2a). **P32** and **P36** lost their activity completely toward the other strains in the presence of salts. All of the other analogs completely lost their activity in the presence of NaCl against all of the microbial strains tested (Table 1). It is mention-worthy that the template peptide P4 also had a salt sensitive activity toward the microbes. Salt tolerance of the most active peptide **P36** against *P. aeruginosa* was further performed in the presence of some physiologically lesser abundant salts like $MgCl_2$ and $CaCl_2$ (Figure S24). Activity of **P36** against *P. aeruginosa* was completely retained in the presence of $CaCl_2$ (20 μM) while it was partially compromised in the presence of $MgCl_2$ ($MIC_{99\%} \sim 60$ μM). However, even being compromised in the presence of $MgCl_2$, **P36** retains a moderate antimicrobial activity.

In summary, from the above discussion, it might be concluded that the activities of the different analogs were dependent on the specific microbial species. This was not surprising, as the membranes of different microbial species were quite unique and most of the cationic AMPs manifested their action through membrane interactions. The designed analogs were most potent against *P. aeruginosa*. Decrease in the length of the side chain of the charged amino acid residue led to the increase in the activity of the analogs as seen in the Orn and Dab substituted peptides. However, upon decreasing the side-chain length too much as in Dap substituted peptides, there was a loss in activity which could be recovered partially by the second type of substitution of Leu to Nle. Though Leu and Nle have the same hydrophobicities, the length of the side chains in Nle being longer compared to Leu improved the activity. In the cases of peptides **P31** or **P32**, where the charged side chain was longer, there was effective interaction with the microbial membrane already leading to high activity. Thus, in those cases a second type of mutation of Leu to Nle did not improve the activity further. Additionally, in **P34**, where the hydrophobic–hydrophilic balance was identical to **P4** but the length of the hydrophobic chain was varied; the peptide either had diminished or lost activity against the different microbes. This indicated that, in addition to the optimum hydrophobic hydrophilic ratio, the antimicrobial activity depended on the length of the side chains in being able to make the best interaction with the microbial cell membrane.

P32 and **P36** were found to be the most active peptides against all of the strains tested, with best activity against *P. aeruginosa*. Additionally, **P36** showed salt tolerant activity against *P. aeruginosa*. *P. aeruginosa* is a multidrug resistant opportunist pathogen that causes diseases in plants, animals, and humans. The organism causes serious infection during existing diseases or conditions such as cystic fibrosis or traumatic burns. It is generally problematic to treat infections

https://doi.org/10.1021/acsomega.2c01089
ACS Omega 2022, 7, 15951–15968

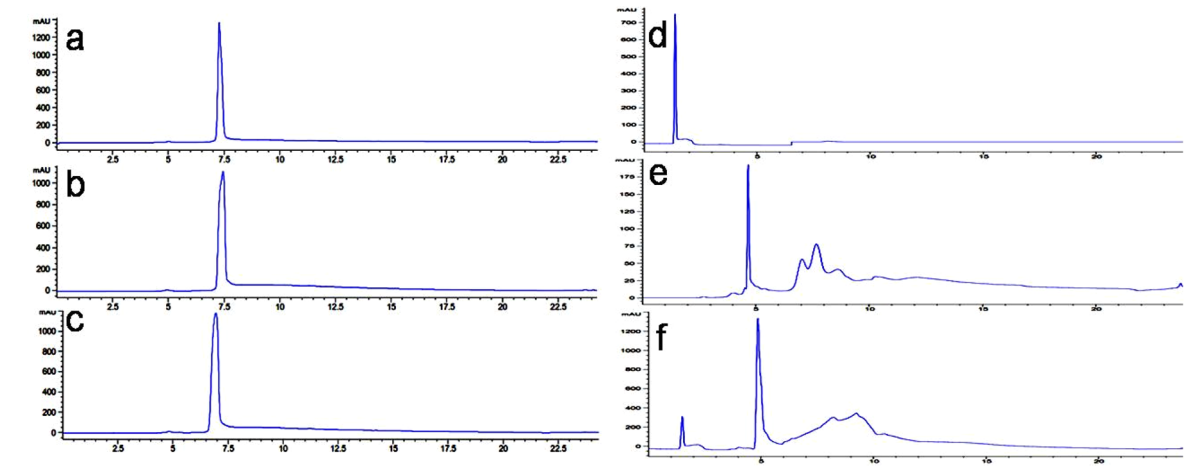

Figure 4. Protease resistance of **P36** and **P4**. Analytical HPLC traces of the **P36** (lLeft panel) and **P4** (right panel), after incubation with an enzyme cocktail (trypsin, chymotrypsin, and proteinase K) for different time intervals. Chromatograms of **P36** and **P4**: (a, d) in the absence of enzymes, (b, e) after 1 h. in the presence of enzyme cocktail, and (c, f) after 12 h in the presence of enzyme cocktail.

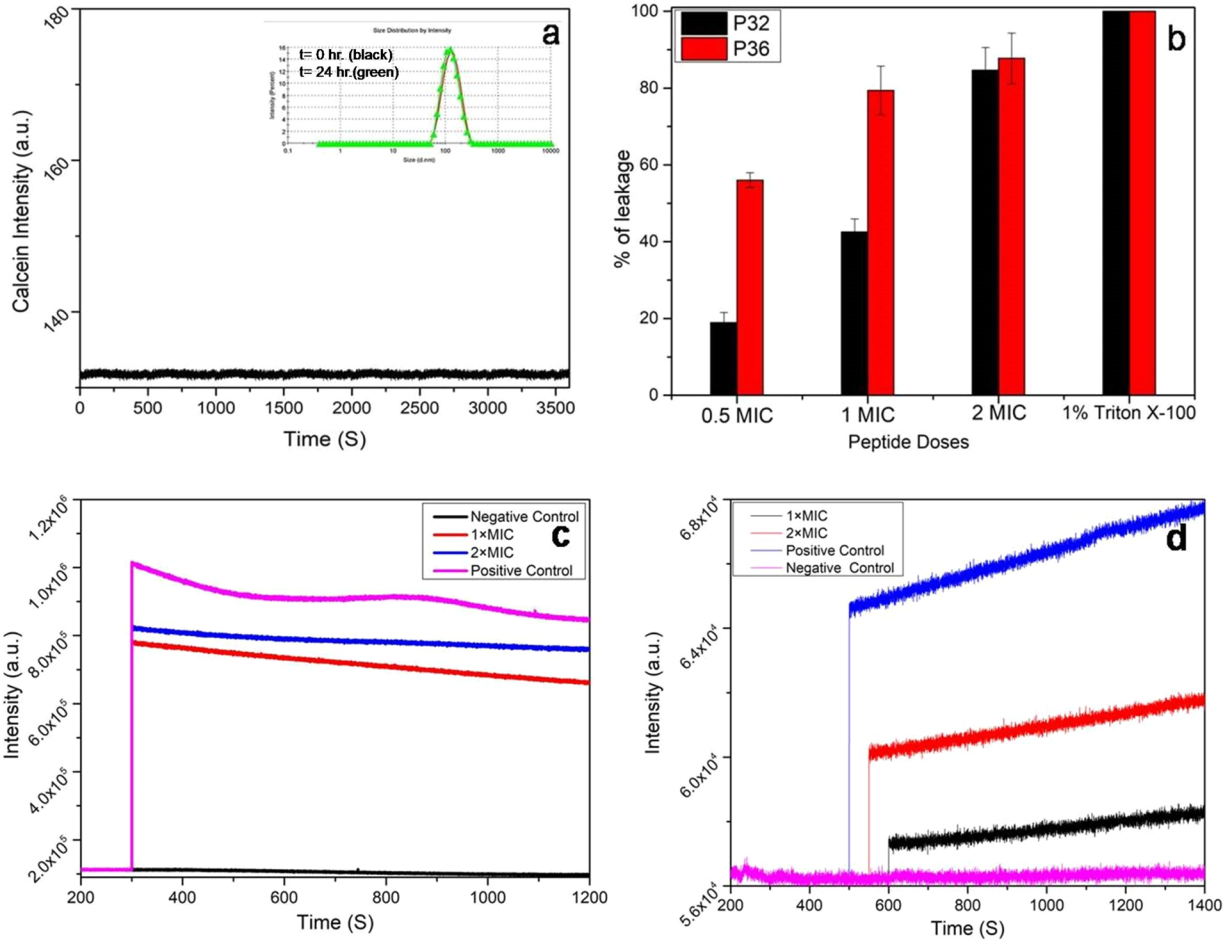

Figure 5. Membrane permeabilization effect of **P32** and **P36**. (a) Structural stability of calcein-entrapped LUVs (3:1 ratio POPE/POPG) in the absence of peptides (inset) monitored over a time period of 3600 s. Unchanged hydrodynamic radius of the LUVs after 24 h (green line) as seen from DLS. Absence of calcein leakage in the untreated LUVs. (b) Calcein dye leakage assay. Bar diagram representing calcein leakage from dye-entrapped LUVs (3:1 ratio of POPE: POPG), a microbial membrane mimic system, upon addition of increasing concentrations of **P32** and **P36**. Triton X-100 (0.1%) was used as the positive control. Time kinetics of (c) NPN and (d) PI uptake after addition of 1× and 2× MIC **P36** to *P. aeruginosa* cells, which indicate the outer and inner membrane permeabilities, respectively. All of the experiments were performed in triplicate.

caused by this organism owing to its intrinsically advanced antibiotic resistance. Though not extremely virulent, this pathogen is capable of extensive colonization and formation of enduring biofilms. Thus, in the later part of the study, we have only focused on the bioactivities, biophysical attributes, and

https://doi.org/10.1021/acsomega.2c01089
ACS Omega 2022, 7, 15951−15968

the mode of action in details against *P. aeruginosa* for the two most active peptides, i.e., **P32** and **P36**.

2.4. Cytotoxicity of the AMPs. Being noncytotoxic to the mammalian cells is one of the basic criteria for being an effective antimicrobial therapeutic. Effects of **P32** and **P36** on the viability of the human embryonic lungs (L132) cell lines were determined using MTT assay. Upon treatment of the cells for 4 h, with 100 μM (concentration greater than $MIC_{99\%}$) **P32** and **P36**, they exhibited a cell viability of ∼90% (Figure 2b), suggesting a very low cytotoxicity at the biologically relevant concentration.

2.5. Hemolytic activity. Being nonhemolytic is yet another basic criterion for any peptide to be used as a therapeutic molecule, and hence the hemolytic activities of **P32** and **P36** against human RBCs were studied. Figure S25 represents the digital image of the hemolytic assay performed against human RBCs at different concentrations of **P32** and **P36** (25, 50, 100, and 200 μM). Incubation of the RBCs with buffer and Triton X-100 were treated as negative and positive controls, respectively. Until 4 h, both **P32** and **P36** were found to be very weakly hemolytic (hemolysis < 10%) until a concentration of 100 μM, which was much greater than their biologically active concentrations.

2.6. Time Course for Bactericidal Activity of P36 on *P. aeruginosa*. To determine the time needed by **P32** and **P36** to express their bactericidal activity against *P. aeruginosa* at its $MIC_{99\%}$, a time course experiment was performed (Figure 3; Figure S26). Cells were incubated with **P32** and **P36** at their respective $MIC_{99\%}$ for different time spans and then spread onto NB agar plates for CFU counting. After overnight incubation of the agar plate, a number of viable cells were calculated. It was observed that almost complete killing of *P. aeruginosa* cells was observed within 45 min for **P36** (Figure 3) and within 60 min for **P32** (Figure S26).

2.7. Protease Resistance of P36. The main bottleneck in the application of the AMPs as therapeutic agents arises from their short serum half-life owing to their protease degradability. To test if our lead peptide **P36** was immune to protease resistance, we checked its chemical integrity upon incubation with a mixture of various proteases such as trypsin, chymotrypsin, and proteinase K in comparison to the template AMP **P4**, using analytical HPLC (Figure 4) and ESI-MS (Figures S27−S32). Peptide **P36** maintained its retention time when injected into the analytical HPLC, even after incubation with the mixture of proteases until 6 h, suggesting its robustness to the protease degradation (Figure 4a−c). This was corroborated from the ESI-MS analysis of the reaction mixture post-incubation with the enzyme cocktail, which contained only intact **P36** (differently ionized, Figures S27−S29) peaks. In contrast, incubation of **P4** with proteases resulted in the appearance of several new peaks at different retention times in the HPLC chromatogram (Figure 4d−f). The protease treated **P4** reaction mixture was analyzed using ESI-MS, which led to the identification of various degraded species (Figures S30−S32). The above results conclusively proved the resistance of **P36** toward enzymatic degradation in comparison to earlier reported all α-amino acid containing **P4**. Further, to investigate if the activity of **P36** was retained upon protease treatment, $MIC_{99\%}$ of protease treated **P36** was studied against *P. aeruginosa*. Figure S33 shows that the activity of **P36** remained unaltered even upon incubating it with proteases for 6 h, confirming that **P36** was indeed protease resistant.

2.8. Mechanism of Action of P36. In order to study the mechanism of action of **P32** and **P36** against *P. aeruginosa* and membrane mimic systems, we performed a series of biophysical experiments as reported below.

2.8.1. Calcein Dye Leakage Assay. In a pursuit to understand the effect of AMPs on the microbial membrane integrity, leakage of calcein dye from POPE/POPG (3:1) large unilamellar vesicles (LUVs) was studied. The composition of the lipids that constitute the LUVs mimic the microbial membrane environment, and thus these LUVs act as microbial cell mimics. DLS studies confirmed the structural stability of the LUVs up to 24 h (Figure 5a, inset). Stability of calcein laden LUVs was also checked by performing a time kinetics of the calcein leakage over 1 h, wherein no detectable calcein fluorescence was observed (Figure 5a). The fluorescence of calcein is not observed when trapped inside the LUVs, while it enhances greatly upon leakage from them. Thus, the enhancement of calcein fluorescence intensity is directly related to the dye leakage from the LUVs and thus membrane disruption. Upon treating the LUVs with 0.5×, 1×, and 2× MIC of **P32**, about 18, 41, and 81% enhancement of calcein fluorescence intensity was observed, while 0.5×, 1×, and 2× MIC of **P36** led to 53, 76, and 85% enhancement of fluorescence signal (Figure 5b). This study clearly indicated a membrane disruptive mode of action for both **P32** and **P36**, with a greater efficiency in the later.

2.8.2. NPN Uptake Assay (Outer Membrane Permeability). Outer membrane permeabilization of *P. aeruginosa* was studied by NPN dye uptake assay. NPN, a hydrophobic dye, is usually excluded by the outer membrane due to permeability barrier from interacting with the membrane lipids. However, disruption of the outer membrane upon treatment with AMPs or other membranolytic agents enables the binding of NPN to the membrane lipids, generating an enhanced fluorescence signal. In the present study, enhancements of 75 and 80% in the fluorescence intensity of NPN were observed upon incubating *P. aeruginosa* cells with 1× and 2× MIC of **P36**, respectively (Figure 5c). Similarly, enhancements of 20 and 80% in the fluorescence intensity of NPN were observed upon incubation of *P. aeruginosa* cells with 1× and 2× MIC of **P32**, respectively (Figure S34). In the negative control experiment, the untreated cells did not show any increase in the fluorescence of NPN, while, in the positive control experiment, Triton X-100 led to 100% enhancement of the fluorescence signal. It can thus be concluded that **P36** causes considerable disruption of the outer membrane of *P. aeruginosa* and much more efficiently than **P32**.

2.8.3. PI Uptake Assay (Inner Membrane Permeability). The inner membrane permeability of **P36** for the *P. aeruginosa* cells was studied using propidium iodide (PI) assay. PI is a fluorophore that generates high fluorescence signal upon intercalating with the bases of DNA. Because PI is impermeable through healthy membrane, and only permeates through compromised membrane, this assay is used to study the inner membrane permeability of the AMPs. Figure 5d shows 20 and 40% increments in intensity of PI upon incubating *P. aeruginosa* cells with **P36** for 0.5 h at its 1× and 2× MIC, respectively. Figure S34 shows ∼15 and 60% increases in the intensity of PI upon using 1× and 2× MIC of **P32**. In contrast, in the negative control, untreated cells did not show any enhancement in the PI fluorescence. This proved that both **P32** and **P36** caused inner membrane permeability

https://doi.org/10.1021/acsomega.2c01089
ACS Omega 2022, 7, 15951−15968

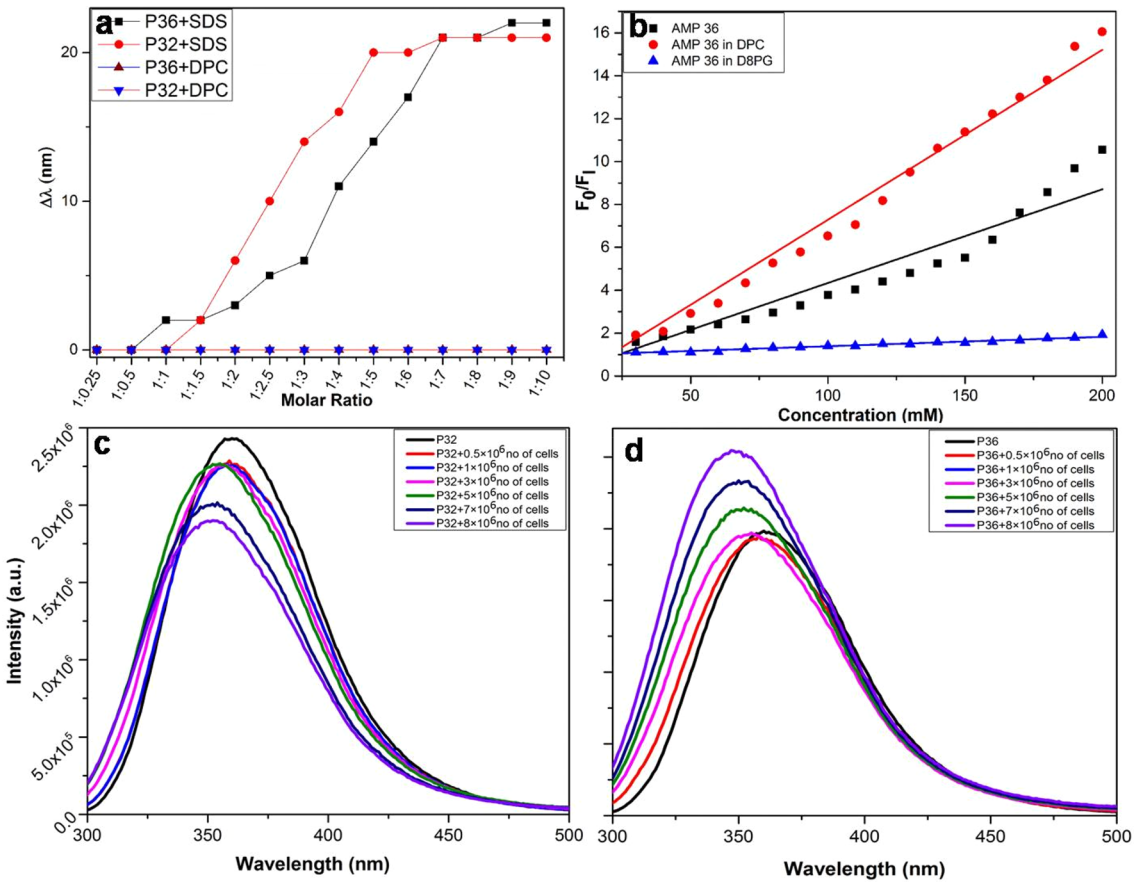

Figure 6. Interactions of **P32** and **P36** with membrane mimics/live membranes. (a) Change in fluorescence emission maxima ($\Delta\lambda$) of Trp residues of **P32** and **P36** in the presence of varying ratios of peptide: lipid (SDS and DPC). A blue shift in the emission maxima occurs for both **P32** and **P36** with increasing concentrations of SDS, a bacterial membrane mimic suggesting an interaction between the two, while there is no change in the fluorescence maxima upon addition of DPC, indicating no interaction between them. (b) Plot of F_0/F_1 against concentration of peptide alone and in the presence of membrane mimics such as D8PG and DPC. Change in the fluorescence emission maxima of the tryptophan fluorescence of (c) **P32** and (d) **P36**, respectively, in the presence of increasing concentration of live *P. aeruginosa* cells.

of the *P. aeruginosa* cells, with the latter being marginally more efficient at the MIC concentrations

2.8.4. Peptide–Membrane-Mimetic/Peptide–Live-Cell Interactions by Fluorescence Spectroscopy. From the above biophysical studies, **P36** has been shown to be highly membrane active. Membrane association is a prerequisite for the membrane activity needed to manifest the antimicrobial activity of AMPs. For understanding the selectivity in the membrane association of **P32** and **P36**, their interactions with the microbial and mammalian membrane mimics and live cells were studied by using intrinsic fluorescence of the aromatic amino acid residue Trp. SDS and DPC micellar systems, containing negative and zwitterionic charges on the surface, respectively, were considered to be microbial and mammalian membrane mimetic systems, respectively.

Upon addition of increasing amounts of SDS micelles to the solutions of **P32** and **P36**, the fluorescence emission of Trp underwent a blue shift of around 22 nm (Figure 6a). This indicated insertion of Trp into the hydrophobic environment of the SDS acyl chains, in turn suggesting an interaction between the peptides and the SDS micelles. Upon similar addition of increasing amounts of DPC micelles to the peptides, no blue shift in the fluorescence emission of Trp was observed, suggesting no interaction between them (Figure 6a). Fluorescence quenching experiments of **P36** alone and in membrane-mimetic environments such as SDS and DPC were performed in the presence of a static quencher such as bis(acrylamide) for understanding the solvent exposure (Figure 6b). The extents of quenching of Trp fluorescence of the free peptide and that in the presence of the membrane-mimetic environment were expressed in terms of Stern–Volmer constant (K_{sv}). It was observed that the K_{sv} values for the peptide alone and the peptide in DPC were higher than that seen in SDS. This indicated that the peptide was much more solvent exposed in DPC, the mammalian membrane mimetic environment, than in SDS, the microbial membrane mimetic environment. Or, in other words, **P36** selectively interacted with the microbial membrane mimetic environment over the mammalian membrane mimetic environment, leading to the lesser exposure of Trp in the former.

Next, in order to understand the interactions of **P32** and **P36** with the live *P. aeruginosa* cell membranes, increasing amounts of cells were added to the peptides while monitoring the Trp fluorescence (Figure 6c,d). Upon increasing the concentration of the cells, an increasing blue shift in the emission maxima was observed for both **P32** and **P36**, which might be attributed to the embedding of Trp in the hydrophobic environment of the microbial membranes. This observation conclusively established the interaction between **P32** and **P36** with *P. aeruginosa* cell membranes.

2.9. Determination of the Thermodynamic Factors in the Binding of P32 and P36 with Lipopolysaccharide.

https://doi.org/10.1021/acsomega.2c01089
ACS Omega 2022, 7, 15951−15968

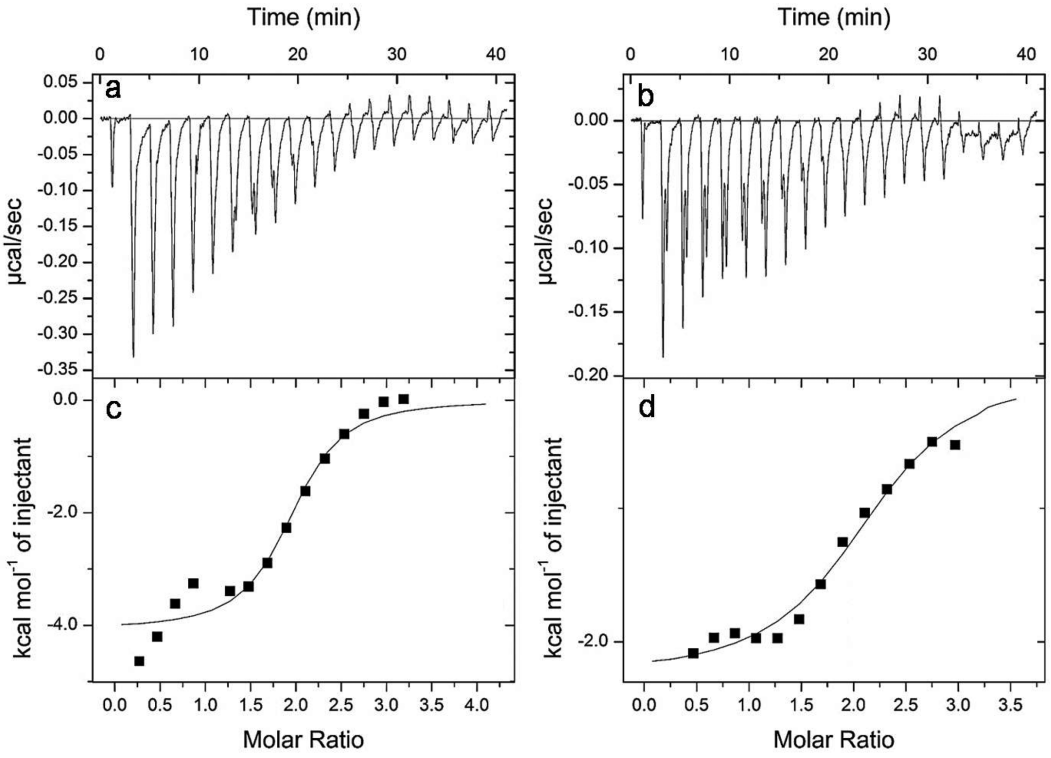

Figure 7. Isothermal titration calorimetry (ITC) for **P32** and **P36** in the presence of LPS (50 μM), a component of the outer leaflet of the bacterial membrane. Exothermic heat of reaction with LPS micelles vs time of interaction for (a) **P32** and (b) **P36**. Plot of enthalpy change per mole of peptide (c) **P32** and (d) **P36** injection with the peptide:LPS molar ratio.

P32 and **P36** exhibited the best activity toward *P. aeruginosa*, a Gram-negative bacteria. The outermost leaflet of the asymmetrical bilayer of the outer membrane of the Gram-negative bacteria is composed of lipopolysaccharide (LPS). Hence, any antimicrobial agent that acts on the Gram-negative bacteria first encounters the LPS layer. We wanted to look at the thermodynamic parameters associated with the interaction between the **P32**/**P36** and LPS through ITC (Figure 7). The isotherm obtained for both **P32** and **P36** indicated a negative enthalpy change or an exothermic reaction with LPS (Figure 7a,b). Gibb's free energies of the interactions were calculated (Table 2). P36 was found to be marginally preferred over P32 towards LPS binding. The peptide binding to LPS is both entropically and enthalpically favoured.

2.10. Peptide–Live-Cell Interaction Studied through Microbial Surface ζ Potential. Interaction of **P36** with the live *P. aeruginosa* cells was studied by monitoring the surface ζ potential of the cells. Microbial cells are negatively charged and hence have a negative surface ζ potential. Upon binding of the cationic peptides to the negatively charged microbial membranes, the surface ζ potential of the cell surface becomes less negative. Thus, a decreasing negative ζ potential is an indication of the peptide–membrane interaction. Upon addition of **P36** to the live cells, the surface ζ potential of the *P. aeruginosa* cells became less negative and plateaued out beyond 1× MIC to about 0 mV (Figure 8a). This observation conclusively proved binding of **P36** to the *P. aeruginosa* cell membrane.

Table 2. Thermodynamic Parameters in the Interaction of P32 and P36 with SDS Calculated from ITC Experiments Performed at 298 K

	peptide	
thermodynamic parameters	**P32**	**P36**
K_A (M^{-1})	1.83×10^5	4.72×10^5
ΔG (kcal·mol^{-1}) = $-RT \ln K_A$	−7.18	−7.74
N (stoichiometry)	2.13	1.90
ΔH (kcal.mol^{-1})	−2.26	−4.08
ΔS (kcal·mol^{-1}·K^{-1})	16.6	12.4
$T\Delta S$(kcal·mol^{-1})	4.95	3.70-
K_D (M)	5.46×10^{-6}	2.12×10^{-6}

2.11. Structure of AMP upon AMP–Membrane-Mimic/AMP–Live-Cell Interactions Using CD. The secondary structure of the peptides often plays an important role in the peptide–membrane interactions and hence the activity of the peptides. We wanted to study the structure of the two most active peptides **P32** and **P36** in free state and in the presence of membrane-mimetic systems. Figure S35 shows the change in molar ellipticities of **P32** and **P36** in water, 50% TFE (a helix promoting solvent), SDS micelles, and DPC micelles. Both peptides adopted a random coil conformation in water and also in the presence of the different membrane-mimetic environments. This suggested that the peptides bound to the membranes mimics as random coils.

We further wanted to study the **P36**–*P. aeruginosa* interactions through circular dichroism (CD) spectroscopy. CD was performed on **P36** alone in phosphate buffer and on **P36**–*P. aeruginosa* cell mixture at different time points (Figure 8b). Later, fresh **P36** was added to the peptide–live-cell mixtures and CD was studied. **P36** formed a random coil conformation with a negative peak at 200 nm. The live *P. aeruginosa* cells in phosphate buffer at pH 7.4 showed a positive peak at 200 nm and a negative peak at around 228 nm. Upon addition of 1× MIC of **P36** to the cells, the positive and

https://doi.org/10.1021/acsomega.2c01089
ACS Omega 2022, 7, 15951−15968

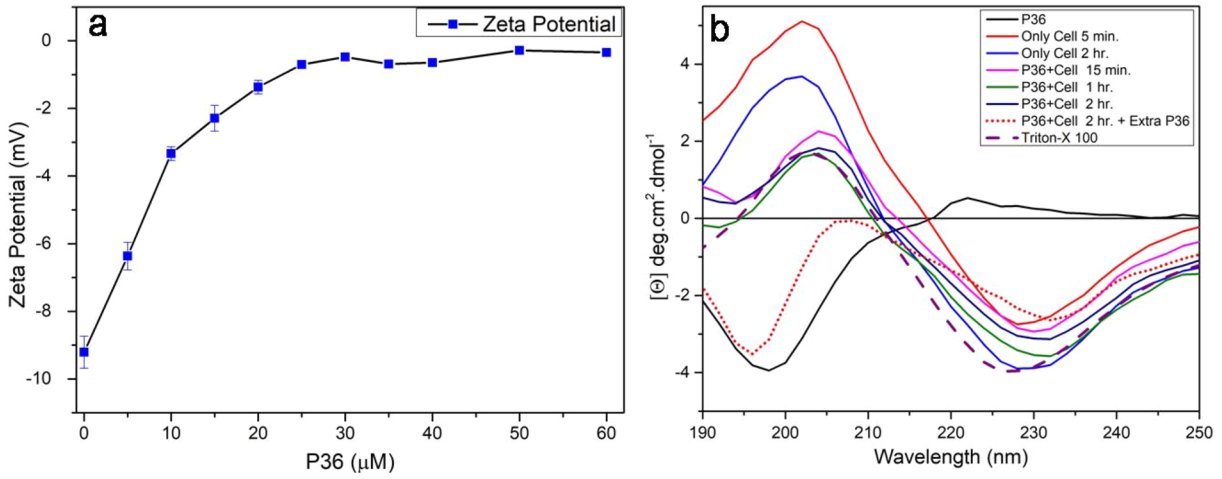

Figure 8. (a) Surface ζ potential of live *P. aeruginosa* cells upon addition of increasing concentration of **P36**. (b) CD spectra of **P36** alone in phosphate buffer and in the presence of live *P. aeruginosa* cells at different incubation times.

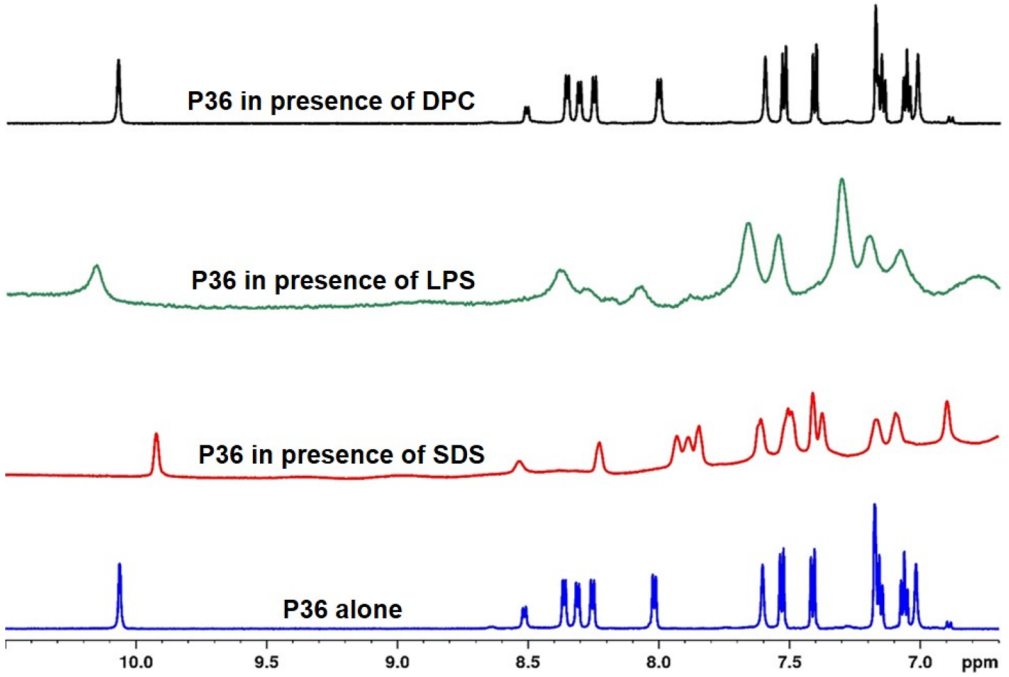

Figure 9. Stacked plots of the NH region of the ^{1}H NMR spectra of **P36** (1 mM) alone and in the presence of SDS, LPS, and DPC. Broadening of the line widths and the change in the chemical shifts of the peptide signals in the presence of SDS and LPS indicate interaction between them. Unchanged line widths and the chemical shifts of the peptide in the presence of DPC suggest absence of interaction between them.

the negative CD peaks red-shifted to around 205 and 232 nm, respectively. The positive peak intensity was significantly diminished upon addition of **P36**. This was due to the cancellation of a positive peak from the *P. aeruginosa* cells by the negative peak of **P36**. The negative peak of the cells remained almost similar in intensity in the **P36**:*P. aeruginosa* complex due to absence of any peaks from **P36** in this region. The slight red shift in the peak positions of the final **P36**−*P. aeruginosa* system was owing to the interactions between them. The spectra of the **P36**−*P. aeruginosa* mixture remained almost unchanged from 15 min to 2.5 h, indicating completion of interaction within the first 15 min. Upon addition of fresh **P36** after 2.5 h, a negative peak reappeared at 195 nm, suggesting random coil conformation of the freshly added **P36** in addition to the negative Cotton effect peak at ∼230 nm from the **P36**−*P. aeruginosa* complex. The positive peak of the **P36**:*P. aeruginosa* cell complex was not observed as it was canceled by the negative peak of the free peptide. The peptide added in the second slot was excess in comparison to the cells, which were already completely complexed with the peptide added in the first slot. Hence, the peak due to the free **P36** reappeared in this case. Thus, we concluded that the peptide existed as random coil in the free state as well as in the live *P. aeruginosa* cell bound systems. Adoption of random coil conformation in the presence of membrane mimics and live cells may be attributed to the very small size of the AMPs.

2.12. P36−Membrane-Mimic Interaction through NMR. Next, we wanted to study the interaction of **P36** with (a) SDS, the microbial membrane mimic; (b) LPS, constituent of the Gram-negative microbial membrane; and (c) DPC, the

https://doi.org/10.1021/acsomega.2c01089
ACS Omega 2022, 7, 15951−15968

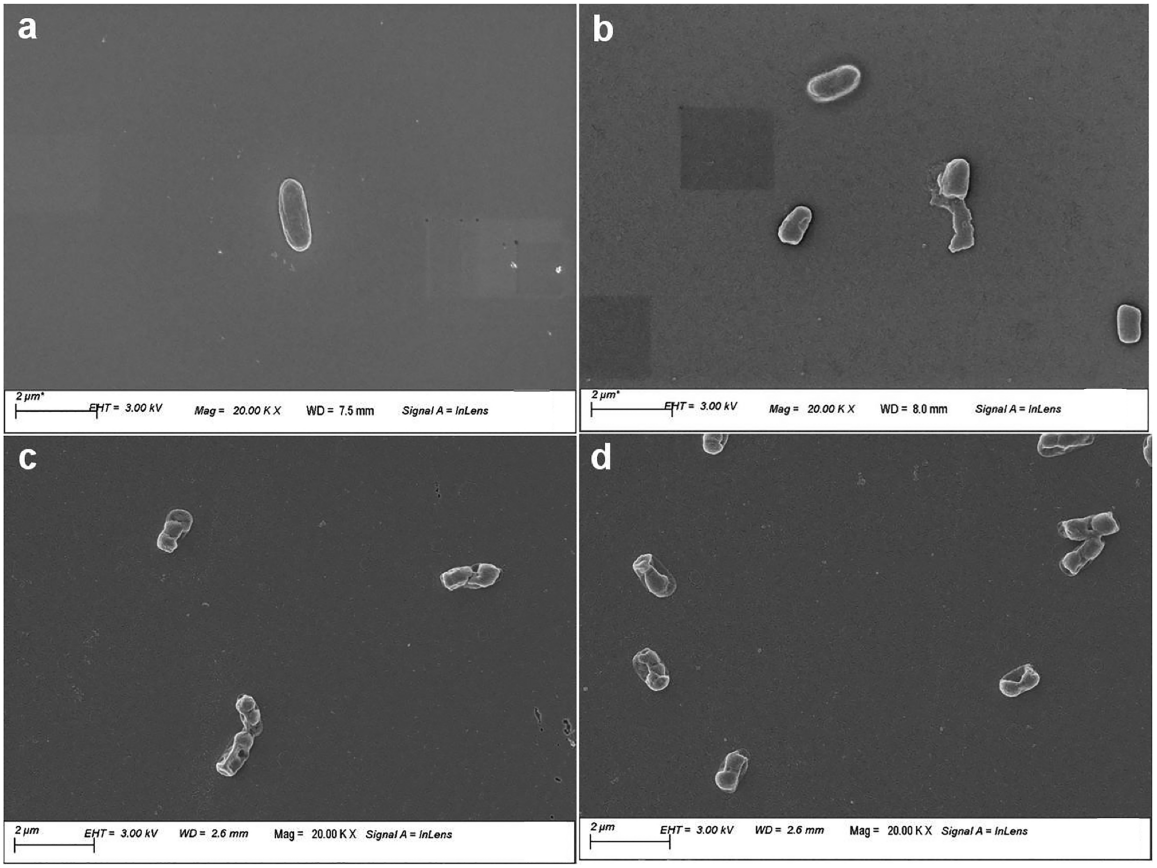

Figure 10. Field emission scanning electron microscopic (FESEM) images of the *P. aeruginosa* cells in the absence and presence of **P36**. (a) Negative control and (b) positive control in the presence of 10 μM Polymixin B. Considerable deformation in cellular morphology observed upon incubation of cells with (c) 1× MIC and (d) 2× MIC of **P36**.

mammalian membrane mimic using NMR. Figure 9 shows the stacked plots of the aromatic region of the ^{1}H NMR spectra of **P36** (1 mM) in 10% D_2O (containing 10 mM phosphate buffer, pH 6.5) and in the presence of membrane-mimetic environments such as SDS, LPS, and DPC. The sharp NMR signals of **P36** became broad in the presence of SDS and LPS, while it remained unaffected in the presence of DPC. Broadening of the NMR signals was a clear indication of the interaction between **P36** and SDS and LPS. Unchanged line widths of **P36** in the presence of the DPC micellar system suggested the absence of interaction between them. These observations conclusively explained the high antimicrobial potency of **P36** against the *P. aeruginosa* in contrast to its noncytotoxicity toward mammalian cells.

2.12.1. Live-Cell NMR. To understand the details of the mechanism of action of **P36** on *P. aeruginosa* cells, we performed a real time NMR experiment with cells added to the peptide (Figure S36). Line width broadening of all of the signals of the peptide was observed upon incubation with the cells, due to the increase in the t2 relaxation time, suggesting an interaction between **P36** and the live cells. Additionally, new peaks attributed to the leaked metabolites from the lysed, wounded, and dead cells were observed as early as 30 min. The time kill kinetics of bactericidal activity of **P36** against *P. aeruginosa* cells, which had earlier shown considerable killing within 30 min of incubation, corroborated with the NMR observation. The appearance of the metabolite peaks supported the previous biophysical studies and indicated the membranolytic mode of action for **P36**.

2.13. Microscopic Visualization of the Membranolytic Mechanism of Action of P36. In order to visualize the effect of **P36** on the membrane integrity and the morphology of *P. aeruginosa* cells, field emission scanning electron microscopy (FESEM) was performed. *P. aeruginosa* cells were incubated with the **P36** at their 1× and 2× MIC concentrations to study the peptide-mediated deformation and cell lysis. Cells not treated with **P36** retained their healthy morphology with a smooth outer membrane, while the cells treated with Triton X for 4 h showed complete disruption of the cellular morphology and the presence of cell debris (Figure 10a,b). Upon addition of 1× and 2× MIC concentrations of **P36** to the *P. aeruginosa* cells, cellular morphology was severely deformed accompanied by the disruption of the cell membrane (Figure 10c,d).

2.14. Atomistic Visualization of P36 Structure and Membrane Interaction: Insight from MD Simulations. MD simulations of the free peptides (**P36**, **P32**) showed that the peptides remained as a random coil along the MD trajectory (Table S5), in lines with the CD experiment. SDS micelle is a popular mimic of the bacterial membrane[70−72] and was adopted for simulation studies in this work. No secondary structure of the peptide was attained in response to SDS micelle binding (Table S5). Micelle structure (eccentricity, micellar radius) was independent of peptide binding (Table S5). Noticeable structural features observed from the MD structure of the **P36**−SDS complex were as follows: (1) The peptide laid over the surface of the micelle with noticeable local deformation (∼11 Å width and ∼13 Å deep peptide binding pocket, Figure 11a) of the micelle surface. (2) Trp3

https://doi.org/10.1021/acsomega.2c01089
ACS Omega 2022, 7, 15951−15968

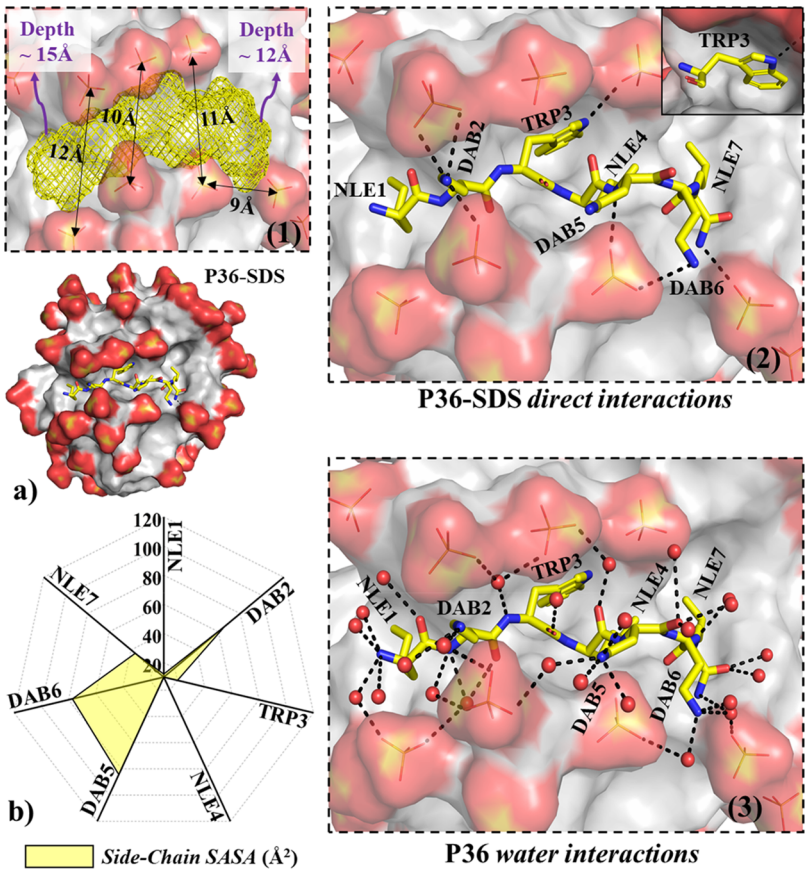

Figure 11. (a) Representative snapshot of **P36**:micelle (SDS) complex (without ions and water) after 50 ns of MD. Peptide **P36** is shown as yellow sticks (nitrogen, blue; oxygen, red) and SDS micelle shown as surface representation. Zoomed-in views of the peptide:micelle binding pockets are shown in the black-broken-line boxes: (1) SDS micelle pocket hosting the peptide shown as yellow mesh (dimensions: width, ∼10−12 Å; depth, ∼12−15 Å). (2) Direct peptide:micelle interaction. Trp3 side chain is found to be buried in a dry (no waters found within 3.4 Å of Trp side chain) hydrophobic core of the micelle that satisfied the hydrogen bonding requirement of the indole−NH, forming direct interaction with sulfate of SDS (shown explicitly in the solid box). Hydrophobic side chains (Nle1, Nle4, and Nle7) are also found to be buried in the SDS core. Positively charged side chains (Dab2, Dab5, and Dab6) are exposed to bulk water and establish direct salt bridges with negatively charged SDS surfaces. (3) Peptide water interactions, in which peptide satisfied its backbone hydrogen bonding requirement by involving waters. Water-mediated peptide, in which micelle interaction was observed. SDS sulfates within 3.4 Å of the peptide are shown explicitly in sticks form (sulfur, yellow; oxygen, red). Black broken lines represent interactions (distance between two heavy atoms < 3.4 Å). Hydrogens are not shown for clarity. (b) Side-chain solvent accessibility of **P36** estimated by calculating the solvent-accessible surface area (SASA). The SASA was averaged over the last 30 ns of the 50 ns MD trajectory. The solvent exposure (yellow area in the net plot) is shown with broken lines of constant exposure in the net plot.

and Nle4 side chains were found to be on the same side relative to peptide backbone. (3) Trp3 was found to be buried in the dry hydrophobic core of the SDS micelle, in lines with the experimentally observed shift in the emission maxima of the tryptophan fluorescence (Figure 6a,c). No water was found within 3.4 Å of the Trp3 side chain. The hydrogen bonding requirement of the polar "-NH" of the indole ring of Trp3 was found to be satisfied by establishing direct interaction with the oxygen of the terminal sulfate of SDS (Figure 11a). (4) Hydrophobic side chains of Nle1 and Nle4 were found to be more buried relative to Nle7 in the hydrophobic core of SDS micelle (Figure 11a,b). (5) High solvent exposure was observed for the positively charged side chains of Dab2, Dab5, and Dab6 (Figure 11b). The interaction network of the positively charged terminals of Dab2, Dab5, and Dab6, were of three kinds: (I) direct interaction with the negatively charged sulfate oxygens of SDS (Figure S39), (II) water-mediated interaction with SDS, and (III) interaction with the bulk water. (6) The peptide backbone satisfied its hydrogen bonding requirement by forming H-bonds with water molecules or sulfates of the SDS micelle or both (Figure 11a; Figure S40). The above structural observations were robust features of our MD simulations (confirmed from six independent MD runs differing in the initial structural model and initial velocities; see Experimental Section). A similar observation was confirmed from **P32** simulations in the presence of SDS micelles (Figures S37 and S38).

P32 and **P36** binding to the SDS micelles were found to be significantly faster relative to zwitterionic DPC micelles, due to obvious electrostatic reasons (Figure S41). **P36** was able to bind to the DPC micelle surface after 38 ns of dynamics, much slower relative to the initial SDS binding event which took place within 1−3 ns (Figure S44). The results indicated that electrostatic interactions were crucial for initial peptide:micelle binding kinetics. Although the kinetics of the initial peptide binding event depended on the nature of the micelles (SDS or DPC), the interaction network between the peptide and micelle in the final equilibrated peptide:micelle complex was more or less similar between peptide:SDS and peptide:DPC micelles (Figures S37−S41).

https://doi.org/10.1021/acsomega.2c01089
ACS Omega 2022, 7, 15951−15968

3. CONCLUSIONS

We have successfully designed a lead protease resistant AMP **P36**, with high salt tolerant potency against Gram-negative bacteria *P. aeruginosa*. **P36** manifested noncytotoxic and nonhemolytic behavior against mammalian cell lines. We established the membranolytic mode of action of **P36** using several biophysical, spectroscopic, and microscopic tools. The study illustrated that the antimicrobial activity of AMPs was dependent on the hydrophobic−hydrophilic balance and the length of the side chains of amino acid residues, disruption of which led to the loss in activity or increase in the cytotoxicity. In this work, we have overcome several significant shortcomings of the AMPs, viz., the salt induced inactivation of the bioactivity protease degradability and cytotoxicity which limit their therapeutic potential and applicability. Antimicrobials such as **P36** hold immense potential for being commercialized as antimicrobial agents of the future.

4. EXPERIMENTAL SECTION

Peptide synthesis, purification, and characterization details for the peptides **P31**−**P37** have been described in detail in the Supporting Information (SI).

4.1. Microbroth Dilution Assay. Antimicrobial activity of the peptides was studied using standard microdilution broth assay.[58] The mid log-phase cultures of *P. aeruginosa*, *K. pneumoniae*, and *S. aureus* were obtained from overnight-grown cultures of the respective microbes. The cell suspensions were centrifuged at 6000 rpm for 5 min. Cell pellets were washed three times each with 10 mM phosphate buffer (pH 7.4) alone or in the presence of (a) 150 mM sodium chloride (NaCl), (b) 1.25 mM magnesium chloride ($MgCl_2$), and (c) 1 mM calcium chloride ($CaCl_2$). Thereafter, the cell pellets were resuspended in the same buffers to obtain a cell suspension of 10^5 CFU/mL. The reaction was performed in a 96 well plate, where 50 μL of the cell suspension was incubated with different concentrations of peptide (ranging from 1 to 200 μM), prepared from 1 mM peptide stock in phosphate buffer (pH 7.4). The reaction was incubated at 310 K for 4 h. A negative control containing only cell suspension and a positive control containing 1 μM Polymyxin B with cell suspension were maintained. Next, 150 μL of suitable medium was added to each well and the reaction was incubated overnight with constant shaking at 310 K temperature. Absorbance of the culture was monitored at 630 nm to monitor microbial growth. The positive control Polymyxin B was used to normalize all of the other readings. The peptide concentration at which 99% growth inhibition was observed served as its $MIC_{99\%}$. All experiments were performed in triplicate.

The assay was also performed with **P36** incubated with an enzyme cocktail (trypsin, chymotrypsin, and Proteinase K) for 4 h and subsequently quenched, using the same method as explained above.

4.2. Cell Viability Assay. Cell viability effects of the most active peptides were studied using MTT assay. L132 cells were seeded into a 96 well plate at the density of 10^4 cells/well. After incubating the cells overnight, they were treated with different concentrations (0−300 μM) of **P32** and **P36** for 24 h. Subsequently, MTT (0.3 mg/mL) reagent in DMEM was added, the reaction was incubated for 3 h, and the formed formazan crystals were solubilized by adding 200 μL of DMSO. Cell viability was calculated by measuring absorbance at 570 nm by using a Tecan plate reader.

4.3. Hemolytic Assay. Fresh human erythrocyte cells (RBC) were collected in EDTA vials. RBCs were pelleted upon centrifugation at 8000*g* for 10 min at 4 °C, followed by washing with PBS (pH = 7.4) three times. Cells were resuspended in PBS buffer at pH 7.4 to a final concentration of 2×10^8 cells/mL. The cells were incubated with Triton X and various concentrations of peptides (until 100 μM), for 4 h at 37 °C while shaking. The incubated samples were centrifuged at 8000*g* for 10 min at 4 °C. RBC lysis and heme release were quantitatively estimated by monitoring the optical density of the supernatant solution at 414 nm. Heme released upon treatment with 1% Triton X-100 was taken as 100%, and the data from other experiments were normalized against it. All of the experiments were performed in triplicate. Digital photographs of the centrifuged eppendorfs were taken. The color of the supernatant solution indicated the extent of hemolysis qualitatively.

4.4. Time Course of Bactericidal Activity. Overnight-grown culture of *P. aeruginosa* was centrifuged at 6000 rpm for 5 min, and the pellet was washed three times with 10 mM phosphate buffer (pH 7.4). Thereafter, the pellet was resuspended to obtain 10^5 CFU/mL suspension of cells. A 50 μL aliquot of bacterial cell suspension was incubated with MIC of **P32** and **P36** at 310 K for different time intervals (5−120 min). After each incubation time, a 5 μL aliquot was taken from each reaction volume and diluted with the same amount of buffer. The reaction mixture was then spread onto the NB agar plates. The plates were incubated overnight at 310 K, and CFU counting was done. All experiments were performed in triplicate.[61]

4.5. Proteolytic Stability Assay. *4.5.1. HPLC Experiment.* A 10 mM amount of **P4** and 10 mM **P36** were treated with a 1:1:1 mixture of enzymes trypsin, chymotrypsin, and protease K (0.3 mg/mL) at 37 °C for 0−6 h. After incubation, 50 μL of reaction solution was taken and mixed with 50 μL of acetonitrile with 1% TFA at 4 °C and kept for 15 min to inactivate the enzymes. The mixture was then diluted with HPLC grade water, and 20 μL was injected onto the C18 reverse-phase column for HPLC analysis. Samples were eluted by a linear gradient of 10−100% CH_3CN/H_2O in 0.1% TFA at a flow rate of 1 mL/min for 25 min. The UV absorbance of the eluted peptides was detected at 214 and 280 nm with a UV monitor.

4.5.2. Mass Spectrometry. In order to determine the chemical integrity of the most active peptides **P4** and **P36** upon protease degradation, a mass spectrometric analysis of the peptide−enzyme reaction mixture, post-incubation, and the subsequent deactivation of the enzymes were carried out on an Agilent-Q-TOF 6500 instrument equipped with Mass Hunter workstation software in the electrospray ionization positive mode.

(a) In order to see if **P36** retained its activity upon incubation with the proteases, MIC of the enzyme incubated **P36** against *P. aeruginosa* was delineated (Figure S33). **P36** was shown to retain most of its activity even after protease treatment, proving the protease resistance of the peptides.

4.6. Calcein Leakage Assay. To prepare an anionic bacterial membrane-mimicking model, LUVs were made from 1-palmitoyl-2-oleoyl-*sn*-glycero-3-phosphoetanolamine (POPE) and 1-palmitoyl-2-oleoyl-*sn*-glycero-3-phosphoglycerol (POPG) in 3:1 ratio, with a final concentration of 2 mg/mL.

https://doi.org/10.1021/acsomega.2c01089
ACS Omega 2022, 7, 15951−15968

All lipid mixtures were dissolved in chloroform. A lipid film was prepared by passing N_2 gas over it and lyophilizing overnight. Calcein-entrapped vesicles were prepared, thereafter, by hydrating the lipid films with 70 mM calcein (in 10 mM Tris-HCl buffer, pH 7.4). The reaction mixture was vortexed, followed by five freeze−thaw cycles. During the freeze−thaw cycles, liquid nitrogen and hot water (60 °C) were used for freezing and thawing, respectively. To prepare large unilamellar vesicles, calcein-entrapped vesicles were passed through a mini extruder (Avanti Polar Lipids, Alabaster, AL) using two-stacked polycarbonate membrane filters of 100 nm pore size for 27 times. Subsequently, the sample was passed through a gel-filtration-based hydrated Centrisep-spin column by centrifuging at 3000 rpm for 2 min, to remove the free calcein.

Calcein release from 20 μM dye-entrapped liposomes in 600 μL of extravesicular buffer (10 mM Tris, 100 mM NaCl, pH 7.4) was determined by monitoring the emitted fluorescence at 520 nm from liposome dispersion. A Hitachi F-7000 FL spectrometer with a slit width of 2.5 nm was used to monitor the fluorescence. After the stabilization of calcein fluorescence, peptide was added in increasing concentrations and fluorescence enhancement was measured after 5 min of each addition. An absolute leakage of calcein from the LUVs was obtained by disrupting the liposomes at the end of each experiment by addition of 0.1% per volume of Triton X-100. All measurements were performed in triplicate at 298 K. An independent control, containing only 0.1% per volume of Triton X-100, was added to calcein loaded LUVs. This ascertained the maximum disruption and calcein release possible. Similar results were obtained in both the cases.

Percent leakage was calculated using the equation below:

$$\text{percent leakage} = [(F - F_o)/(F_T\text{-}F_o)] \times 100\%$$

where F, F_o, and F_T were (1) fluorescence intensity after addition of peptide, (2) basal fluorescence intensity, and (3) maximum fluorescence intensity obtained after addition of 0.1% per volume of Triton X-100, respectively.

4.7. Assay of Membrane Permeabilization. *4.7.1. Inner Membrane Permeabilization.* The mid-logarithmic phase of *P. aeruginosa* cells was obtained from overnight-grown cultures. The cells were pelleted, and the cell pellet was washed in sodium phosphate buffer (pH 7.4) and resuspended in the same to obtain a concentration of 10^6 CFU/mL of *P. aeruginosa* cells. A 10 μM amount of propidium iodide dye was added to 1 mL of the cell suspension and incubated at room temperature for 30 min under shaking conditions. The fluorescence of the dye was measured at 298 K for 1500 s at an excitation wavelength of 535 nm (slit width, 10 nm) and emission wavelength of 617 nm (slit width, 10 nm) using the Hitachi F-7000 FL spectrophotometer. The fluorescence intensity of the free cell suspension was monitored for any fluctuations in the intensity to test the stability of the cells. After a stable intensity was obtained, **P36** and **P32** were added to the bacterial suspension at different concentrations (1× or 2× MIC). An increase in dye fluorescence suggested the permeabilization of the inner membrane. Peptide induced permeabilization of the inner membrane allowed entry of PI into the cells, which bound with the DNA resulting in an increase of the fluorescence intensity.

4.7.2. Outer Membrane Permeabilization. NPN uptake assay was performed to determine the outer membrane permeabilization ability of **P36** and **P32**. An overnight-grown culture of *P. aeruginosa* cells was washed and resuspended in 10 mM sodium phosphate buffer (pH 7.4) to a final cell concentration of 10^6 CFU/mL. The fluorescence of the dye in the presence of cells alone was monitored for 20 min at room temperature to study the stability of the cells. **P36** and **P32** were added with increasing concentrations (1× and 2× MIC) to a cuvette containing 1 mL of cells and 10 μM NPN. Thereafter increased fluorescence after peptide addition, was monitored for 20 min using the HORIBA JOBIN YVON Fluoromax-4 spectrometer at an excitation wavelength of 350 nm (slit width, 5 nm) and emission wavelength of 410 nm (slit width, 5 nm) to determine the NPN uptake.

4.8. Fluorescence Experiments. *4.8.1. Blue Shift Experiment. 4.8.1.1. Shift in Presence of Membrane Mimetics.* The intrinsic tryptophan fluorescence of **P32**/**P36** was utilized to analyze their interaction with the membrane mimics. SDS and DPC were taken to mimic bacterial and mammalian membranes, respectively. **P32**/**P36** at their respective MIC concentrations (against *P. aeruginosa*) were titrated against increasing concentration of SDS and DPC at 25 °C. The molar ratio of the peptide:peptide-mimic systems was varied from 1:0.25 to 1:10. The change in the fluorescence emission intensity (fluorescence emission range, 295−520 nm) of Trp against an excitation wavelength of 280 nm was monitored on the HORIBA JOBIN YVON Fluoromax-4 spectrophotometer.[61]

4.8.1.2. Shift in Presence of Live Cells. Intrinsic tryptophan fluorescence was utilized to analyze the interaction between the peptide and live *P. aeruginosa* cells. *P. aeruginosa* cells were collected, washed, and resuspended in 10 mM phosphate buffer (pH 7.4). Cells (5 μL) were added (stock, 10^8 CFU/mL) in subsequent steps to the **P32** and **P36** solutions. Trp fluorescence emission was monitored (for an excitation wavelength of 280 nm, excitation and emission slit widths of 2.5 nm) only for **P32** and **P36** and in the presence of live *P. aeruginosa* cells.

4.8.2. Solvent Sccessibility. Intrinsic fluorescence of tryptophan of **P36** in 10 mM phosphate buffer in the absence and presence of D8PG (microbial membrane mimetic) and DPC were recorded by using the HORIBA JOBIN YVON Fluoromax-4 spectrophotometer. The intrinsic Trp fluorescence emission spectra of **P36** (10 μM) upon titration with increasing concentration (from 10 to 200 μM) of D8PG and DPC were measured at an excitation wavelength of 280 nm and excitation/emission slit of 2.5 nm, over an emission spectral range of 295−520 nm. All of the fluorescence experiments were performed at 25 °C in a quartz cuvette of 1 cm path length. Fluorescence quenching experiments was used to determine the solvent accessibility of **P36** in the vicinity of D8PG. Acrylamide, a static quencher, was added to the peptide−D8PG complex as well as free peptide solution up to a final concentration of 0.2 M. The resultant fluorescence intensity of the peptide was analyzed by fitting to the Stern−Volmer equation.

$$F_0/F = 1 + K_{SV}[Q]$$

where F_0 denotes the initial fluorescence intensity in the absence of the quencher, F stands for the fluorescence intensity at each quencher concentration, and [Q] denotes concentration in terms of molarity. K_{sv} represents the Stern−Volmer quenching constant expressed in M^{-1} calculated from the above equation, both in free and bound states of **P36**.[61]

https://doi.org/10.1021/acsomega.2c01089
ACS Omega 2022, 7, 15951−15968

4.9. ITC Experiments. Isothermal calorimetry was performed on MicroCal iTC200 (GE Healthcare) to assess the binding interaction between **P32** and **P36** with lipopolysaccharide (LPS). Peptides and LPS stock solutions were prepared in 10 mM phosphate buffer (pH 7.2). LPS solutions were vortexed for 10 min and sonicated for 5 min before loading into the cell. LPS solution (50 μM) was taken in the cell, and 1 mM concentrations of **P32** and **P36** were taken in the syringe. Peptide concentration was 20 times greater than the LPS concentration. The concentration of LPS used was above its critical micelle concentration (CMC) values (CMC $\sim$ 14 μg/mL or 1.6 μM). The reaction was carried out at 298 K with 20 peptide injections (3 μL each), at an interval of 180 s at 300 rpm stirring speed.[62] A single site binding model was used to elucidate the equilibrium association constant (K_a) and the enthalpy change (ΔH). Basic thermodynamic equations, as given below, were used to determine the Gibb's free energy change (ΔG) and entropy change (ΔS).

$$\Delta G = -RT \ln K_a \quad \text{and} \quad \Delta G = \Delta H - T\Delta S$$

respectively.

4.10. Circular Dichroism Spectroscopy. Solution structure of the peptides was studied using circular dichroism spectroscopy. The spectra of **P31**−**P37** were recorded on a Jasco J-815 spectropolarimeter (Tokyo, Japan). (±)-10-Camphorsulfonic acid was used for calibration of optical rotation. The spectra were measured over a wavelength range of 260 to 190 nm, using a 1 mm path length Suprasil quartz cuvette at a scan rate of 100 nm/min, interval of 0.5 nm, and time constant of 1 s. An accumulation of three scans at 298 K was collected. **P31**−**P37** were dissolved in different solvents such as deionized water, 50% TFE, 30 mM SDS, and 10 mM DPC to generate a 50 μM final peptide solution.

4.11. Live-Cells CD Spectroscopy. Overnight-grown *P. aeruginosa* cells were collected, washed, and resuspended in 10 mM phosphate buffer (pH 7.4) to a final cell count of 5×10^5 cells/mL. Cells (50 μL) were added (stock, 10^8 CFU/mL) to **P36** solution (25 μM, 250 μL), and CD spectra were recorded after different incubation times (until 2.5 h) using a 1 cm quartz cell, 260 to 190 nm measurement range, 100 nm/min scanning speed, 2 nm bandwidth, 4 s response time, and 1.0 nm data pitch up to 2.5 h of incubation at 37 °C. Similarly, the CD spectrum for *P. aeruginosa* cells only was measured under identical conditions. The peptide concentration was 25 μM in 10 mM phosphate buffer (pH 7.4).[63]

4.12. Live-Cells ζ Potential. ζ potential was measured with the help of a Zetasizer Nano ZS 90 instrument (Malvern, U.K.), containing helium−neon laser (633 nm) as a source of light, with the detection at 90° scattering angle at room temperature (28 °C). Overnight-grown *P. aeruginosa* cells were washed three times by DI water and resuspended in the same to obtain a cell suspension of 5×10^5 cells/mL. To minimize the effect of buffer on the ζ potential value, cells were suspended in DI water instead of buffer. **P36** (1 mM stock solution, 5 μL) was added to 1 mL of *P. aeruginosa* cells (5×10^5) at different time intervals, and its ζ potential value was checked after each addition.[64,65]

4.13. NMR Experiments. *4.13.1. NMR in the Presence of Microbial Membrane Mimics (SDS and LPS).* One-dimensional proton NMR for 1 mM **P36** in 90% of 10 mM phosphate buffer (pH 6.5) and 10% D_2O was recorded on a Bruker Avance III 600 MHz NMR spectrometer. ^{1}H NMR was performed for **P36** (1 mM) also in the presence of different membrane-mimetic environments, such as 200 mM perdeuterated SDS (microbial membrane mimetic), 3 μM LPS (Gram-negative bacterial membrane component), and $\geq$2.5 mM DPC micelles (mammalian membrane mimetic).

4.13.2. Live-Cell NMR Experiments. *P. aeruginosa* cultures were grown overnight and used to perform the experiment. The cell suspensions were centrifuged at 6000 rpm for 5 min. Cell pellets were washed three times with 10 mM phosphate buffer at pH 6.5 and later resuspended in the same buffer to obtain a cell suspension containing 10^6 CFU/mL. One-dimensional (1D) proton NMR spectra of 1 mM solution of **P36** in a mixture of 90% of 10 mM phosphate buffer (pH 6.5) and 10% D_2O was recorded on a Bruker Avance III 600 MHz NMR spectrometer. In another experiment, 500 μg of solid peptide **P36** was added to a 500 μL solution of the cells (10^6 CFU/mL), and the mixture was thoroughly vortexed to achieve a final peptide concentration of 1 mM. A series of 1D ^{1}H NMR spectra were recorded at different time points after addition of **P36** to the *P. aeruginosa* cells. The temperature for the experiment was adjusted as per the standard growing temperature of *P. aeruginosa* at 310 K.

4.14. Field Emission Scanning Electron Microscopy. *P. aeruginosa* cells from overnight-grown cultures were pelleted down by centrifugation at 6000 rpm for 5 min, washed thrice, and resuspended in 10 mM sodium phosphate buffer at pH 7.4 to a final number of 10^5 cells/mL. The cell suspensions were incubated with different concentrations (1× and 2× MIC) of **P36** for 4 h at 310 K. Untreated cells were set as the control. Post-incubation, the cells were fixed with 2.5% glutaraldehyde for 1 h at 277 K. Next, the cells were washed twice and resuspended in 20 μL of 10 mM sodium phosphate buffer. A 10 μL aliquot of this cell suspension was spotted on a clean glass slide and was allowed to dry overnight. Thereafter, the slides were washed with 50 and 80% ethanol for 5 min each. The samples were finally air-dried, followed by gold coating and observed under the FESEM (Zeiss Gemini).[65]

4.15. MD Simulations. *4.15.1. Modeling of Peptides (P32, P36) in Water.* The most active peptides **P32** and **P36** (in the presence or absence of micelle) were considered for molecular dynamics simulations. The initial linear models of **P32** and **P36** were generated using PyMOL version 2.4.1 software.[66] N- and C-termini of these peptides were modeled as -NH_3^+ and -$CONH_2$, respectively. A water box of dimensions $60 \times 60 \times 60$ Å^3 was overlaid, keeping the linear peptide model at the center. The overall charge (+4) of the peptide was neutralized by adding four chloride ions. A total of $\sim$21075 atoms were considered for MD simulations of peptides in water. Topology descriptions of the nonstandard amino acids (Dab and Nle) were retrieved from the Swiss Side Chain database.[67]

4.15.2. Modeling of Membrane-Mimetic Systems (SDS/DPC Micelles). CHARMM-GUI Micelle Builder[68] was used to build SDS/DPC micelles. SDS micelle was modeled by including a total of 60 molecules of SDS. The experimental value of the aggregation number was reported to be close to 60. Simulations with 60 SDS molecule is a popular choice for computational analysis.[69−72] The micelle was placed at the center and solvated by overlaying a water box of dimensions $100 \times 100 \times 100$ Å^3. For neutralizing the simulation box, 60 Na^+ counterions were added. A total of $\sim$98230 atoms were considered for MD simulations of SDS in water. DPC micelle was modeled in the same way as SDS. DPC is a neutral zwitterionic molecule; thus, no counterion was added. The

https://doi.org/10.1021/acsomega.2c01089
ACS Omega 2022, 7, 15951−15968

final snapshot produced from the molecular dynamics was considered for studying peptide−micelle interactions.

4.15.3. Simulation Setup for Studying Peptide−Micelle Interaction. First, the center of mass of the model linear peptide (**P32** or **P36**) was initially placed ∼55 Å away from the center of mass of the micelle (SDS or DPC; Figure S1a). The water padding was extended in the peptide direction and the solvated water box of dimensions 100 × 100 × 140 $Å^3$ was subjected to MD simulation (Figure S1b). More than 145530 atoms were considered for MD simulations. To check convergence and ensure efficient sampling, we performed various independent MD replicas differing in the initial setup (setup A, setup B, and setup C: orientations of the peptide relative to micelle) (Figure S1a) as well as in their initial velocities (Table S1).

4.15.4. Simulation Parameters. All of the simulations in this study were performed in GROMACS version 2019 package,[73] with CHARMM36 (version March 2019)[74] as force field parameters. The TIP3P[75] water model was used to model waters. Energy minimization was performed using the steepest descent algorithm (step size = 0.1 Å, 50000 steps). After energy minimization, 200 ps of equilibration was performed (restraining only the micelle and peptide) considering *NVT* ensemble (first 100 ps) followed by *NPT* ensemble. After equilibration, the production run for 50 ns was performed and the last 30 ns was considered for analysis. The simulation parameters adopted for this work are given in Table S2. Coordinates were saved at every 10 ps from the MD trajectories for analysis.

4.15.5. MD Trajectory Analysis. Secondary structural content of the peptides was obtained by processing the MD trajectories using the *gmx dssp* tool.[76] Structural deformation of micelles in response to peptide binding was characterized by estimating the trajectory averaged radius of gyration (R_G) and micelle eccentricity using the *gmx gyrate* tool.[73] SASA (solvent-accessible surface area) values are the geometric estimation of the exposure of molecule surface to the bulk solvent. SASA values were computed by *gmx sasa*[77,78] using a probe radius of 1.4 Å. The *gmx distance*[73] tool was used to plot the distance between the center of mass of the micelle and peptide as a function of simulation time. Peptide−micelle distance and SASA of peptide were obtained from the MD trajectories and plotted using OriginPro,[79] and images were generated using PyMOL visualization software.[66]

■ ASSOCIATED CONTENT

Supporting Information

The Supporting Information is available free of charge at https://pubs.acs.org/doi/10.1021/acsomega.2c01089.

(Figures) MD setup, characterizations by analytical HPLC, HRMS, and ^{1}H NMR, MIC bar diagrams, hemolytic assay, bactericidal time kinetics, live-cell NMR, CD interactions, residue specific solvent exposure, peptide−micelle distance; (tables) peptide physicochemical properties and MD simulations and structural parameters; general procedures for peptide synthesis, purification and characterization, materials, and microbial culture and cell culture details (PDF)

■ AUTHOR INFORMATION

Corresponding Authors

Priyadarshi Satpati − *Department of Biosciences and Bioengineering, Indian Institute of Technology. Guwahati (IITG), Guwahati, Assam 781039, India;* orcid.org/0000-0002-0391-3580; Email: psatpati@iitg.ac.in

Sunanda Chatterjee − *Department of Chemistry, Indian Institute of Technology. Guwahati (IITG), Guwahati, Assam 781039, India;* orcid.org/0000-0001-5068-7208; Email: sunanda.c@iitg.ac.in

Authors

Gopal Pandit − *Department of Chemistry, Indian Institute of Technology. Guwahati (IITG), Guwahati, Assam 781039, India*

Tanumoy Sarkar − *Department of Chemistry, Indian Institute of Technology. Guwahati (IITG), Guwahati, Assam 781039, India*

Vignesh S. R. − *Department of Biosciences and Bioengineering, Indian Institute of Technology. Guwahati (IITG), Guwahati, Assam 781039, India*

Swapna Debnath − *Department of Chemistry, Indian Institute of Technology. Guwahati (IITG), Guwahati, Assam 781039, India*

Complete contact information is available at: https://pubs.acs.org/10.1021/acsomega.2c01089

Author Contributions

S.C. designed the project, G.P. performed most of the experiments (synthesis, purification, characterization the peptides, biological assays, and biophysical (CD, fluorescence) experiments), T.S. performed FESEM experiments and some biophysical experiments, V.S.R did the molecular dynamics simulations, and S.D. performed all of the NMR experiments. S.C. and P.S. analyzed the data and wrote the manuscript.

Notes

The authors declare no competing financial interest.

■ ACKNOWLEDGMENTS

S.C. acknowledges CSIR (Grant 01/(2984)/19/EMR-II) and Department of Biotechnology (Grant BT/PR21251/NNT/28/1067/2016) for funding. G.P., T.S., S.D., and S.R.V. thank IIT Guwahati for funding. FIST is acknowledged for the 500 MHz NMR spectrometer. The computing facility by Biomolecular Simulation Lab (BSL, BSBE Department, IIT Guwahati) and BIF, IIT Guwahati; Param-Ishan supercomputing system, IIT Guwahati; Departmental Instrumental Facility, Department of Chemistry and BSBE, IIT Guwahati; and Central Instrument Facility, IIT Guwahati are gratefully acknowledged. Authors thank Dr. A. P. Bidkar for performing the MTT assay.

■ REFERENCES

(1) Magiorakos, A. P.; Srinivasan, A.; Carey, R. B.; Carmeli, Y.; Falagas, M.; Giske, C.; Harbarth, S.; Hindler, J.; Kahlmeter, G.; Olsson-Liljequist, B.; et al. Multidrug-resistant, extensively drug-resistant and pandrug-resistant bacteria: an international expert proposal for interim standard definitions for acquired resistance. *Clin. Microbiol. Infect.* **2012**, *18*, 268−281.

(2) Delcour, A. H. Outer membrane permeability and antibiotic resistance. *Biochim. Biophys. Acta, Proteins Proteomics* **2009**, *1794*, 808−816.

(3) Van Duin, D.; Paterson, D. L. Multidrug-resistant bacteria in the community: trends and lessons learned. *Infect. Dis. Clin. North Am.* **2016**, *30*, 377−390.
(4) Blair, J.; Webber, M. A.; Baylay, A. J.; Ogbolu, D. O.; Piddock, L. J. Molecular mechanisms of antibiotic resistance. *Nat. Rev. Microbiol.* **2015**, *13*, 42−51.
(5) Sarkar, T.; Chetia, M.; Chatterjee, S. Antimicrobial peptides and proteins: From nature's reservoir to the laboratory and beyond. *Front. Chem.* **2021**, *9*, 691532.
(6) Yu, G.; Baeder, D. Y.; Regoes, R. R.; Rolff, J. Predicting drug resistance evolution: Insights from antimicrobial peptides and antibiotics. *Proc. R. Soc. B: Biol. Sci.* **2018**, *285*, 20172687.
(7) Epand, R. M.; Vogel, H. J. Diversity of antimicrobial peptides and their mechanisms of action. *Biochim. Biophys. Acta, Biomembr.* **1999**, *1462*, 11−28.
(8) Nguyen, L. T.; Haney, E. F.; Vogel, H. J. The expanding scope of antimicrobial peptide structures and their modes of action. *Trends Biotechnol.* **2011**, *29*, 464−472.
(9) Nicolas, P. Multifunctional host defense peptides: intracellular-targeting antimicrobial peptides. *FEBS J.* **2009**, *276*, 6483−6496.
(10) Lohner, K.; Sevcsik, E.; Pabst, G. Liposome-Based Biomembrane Mimetic Systems: Implications for Lipid-Peptide Interactions. In *Advances in Planar Lipid Bilayers and Liposomes*, 1st ed.; Vol *6*; Leitmannova Liu, A., Ed.; Academic Press: Waltham, MA, USA, 2008; pp 103−132. DOI: 10.1016/S1554-4516(07)06005-X.
(11) Yeaman, M. R.; Yount, N. Y. Mechanisms of antimicrobial peptide action and resistance. *Pharmacol. Rev.* **2003**, *55*, 27−55.
(12) Miller, S. I. Antibiotic resistance and regulation of the Gram-negative bacterial outer membrane barrier by host innate immune molecules. *mBio* **2016**, *7*, e01541-16.
(13) Nikaido, H. Molecular basis of bacterial outer membrane permeability revisited. *Microbiol. Mol. Biol. Rev.* **2003**, *67*, 593−656.
(14) Silhavy, T. J.; Kahne, D.; Walker, S. The bacterial cell envelope. *Perspect. Biol.* **2010**, *2*, a000414−a00429.
(15) Snyder, D. S.; McIntosh, T. J. The lipopolysaccharide barrier: correlation of antibiotic susceptibility with antibiotic permeability and fluorescent probe binding kinetics. *Biochemistry* **2000**, *39*, 11777−11787.
(16) Rosenfeld, Y.; Barra, D.; Simmaco, M.; Shai, Y.; Mangoni, M. L. A synergism between temporins toward gram-negative bacteria overcomes resistance imposed by the lipopolysaccharide protective layer. *J. Biol. Chem.* **2006**, *281*, 28565−28574.
(17) LaRock, C. N.; Nizet, V. Cationic antimicrobial peptide resistance mechanisms of streptococcal pathogens. *Biochim. Biophys. Acta, Biomembr.* **2015**, *1848*, 3047−3054.
(18) Maria-Neto, S.; de Almeida, K. C.; Macedo, M. L. R.; Franco, O. L. Understanding bacterial resistance to antimicrobial peptides: From the surface to deep inside. *Biochim. Biophys. Acta, Biomembr.* **2015**, *1848*, 3078−3088.
(19) Matamouros, S.; Miller, S. I. S. Typhimurium strategies to resist killing by cationic antimicrobial peptides. *Biochim. Biophys. Acta, Biomembr.* **2015**, *1848*, 3021−3025.
(20) Gan, B. H.; Gaynord, J.; Rowe, S. M.; Deingruber, T.; Spring, D. R. The multifaceted nature of antimicrobial peptides: Current synthetic chemistry approaches and future directions. *Chem. Soc. Rev.* **2021**, *50*, 7820−7880.
(21) Lee, I. H.; Cho, Y.; Lehrer, R. I. Effects of pH and salinity on the antimicrobial properties of clavanins. *Infect. Immun.* **1997**, *65*, 2898−2903.
(22) Chu, H. L.; Yu, H. Y.; Yip, B. S.; Chih, Y. H.; Liang, C. W.; Cheng, H. T.; Cheng, J. W. Boosting salt resistance of short antimicrobial peptides. *Antimicrob. Agents Chemother.* **2013**, *57*, 4050−4052.
(23) Goldman, M. J.; Anderson, G. M.; Stolzenberg, E. D.; Kari, U. P.; Zasloff, M.; Wilson, J. M. Human β-defensin-1 is a salt-sensitive antibiotic in lung that is inactivated in cystic fibrosis. *Cell* **1997**, *88*, 553−560.
(24) Rothstein, D. M.; Spacciapoli, P.; Tran, L. T.; Xu, T.; Roberts, F. D.; Dalla Serra, M.; Buxton, D. K.; Oppenheim, F. G.; Friden, P. Anticandida activity is retained in P-113, a 12-amino-acid fragment of histatin 5. *Antimicrob. Agents Chemother.* **2001**, *45*, 1367−1373.
(25) Falagas, M. E.; Kasiakou, S. K. Toxicity of polymyxins: A systematic review of the evidence from old and recent studies. *Crit. Care* **2006**, *10*, R27.
(26) Raguse, T. L.; Porter, E. A.; Weisblum, B.; Gellman, S. H. Structure− activity studies of 14-helical antimicrobial β-peptides: probing the relationship between conformational stability and antimicrobial potency. *J. Am. Chem. Soc.* **2002**, *124*, 12774−12785.
(27) Ghosh, C.; Haldar, J. Membrane-active small molecules: designs inspired by antimicrobial peptides. *ChemMedChem* **2015**, *10*, 1606−1624.
(28) Molchanova, N.; Hansen, P. R.; Franzyk, H. Advances in development of antimicrobial peptidomimetics as potential drugs. *Molecules* **2017**, *22*, 1430−1489.
(29) Kumar, P.; Kizhakkedathu, J. N.; Straus, S. K. Antimicrobial peptides: Diversity, mechanism of action and strategies to improve the activity and biocompatibility in vivo. *Biomolecules* **2018**, *8*, 4.
(30) Zhang, Q. Y.; Yan, Z. B.; Meng, Y. M.; Hong, X. Y.; Shao, G.; Ma, J. J.; Cheng, X. R.; Liu, J.; Kang, J.; Fu, C. Y. Antimicrobial peptides: Mechanism of action, activity and clinical potential. *Mil. Med. Res.* **2021**, *8*, 48.
(31) Gentilucci, L.; De Marco, R.; Cerisoli, L. Chemical modifications designed to improve peptide stability: incorporation of non-natural amino acids, pseudo-peptide bonds, and cyclization. *Curr. Pharm. Des.* **2010**, *16*, 3185−3203.
(32) Bottger, R.; Hoffmann, R.; Knappe, D. Differential stability of therapeutic peptides with different proteolytic cleavage sites in blood, plasma and serum. *PLoS One* **2017**, *12*, e0178943−0178957.
(33) Berthold, N.; Czihal, P.; Fritsche, S.; Sauer, U.; Schiffer, G.; Knappe, D.; Alber, G.; Hoffmann, R. Novel apidaecin 1b analogs with superior serum stabilities for treatment of infections by gram-negative pathogens. *Antimicrob. Agents Chemother.* **2013**, *57*, 402−409.
(34) Liang, X.; Liu, K.; Zhao, P.; Zhou, J.; Zhang, F.; He, Y.; Zhang, H.; Fareed, M. S.; Lu, Y.; Xu, Y.; et al. The effects of incorporation of the counterparts and mimics of l-lysine on the antimicrobial activity, hemolytic activity, cytotoxicity and tryptic stability of antimicrobial peptide polybia-MPII. *Amino Acids* **2022**, *54*, 123−135.
(35) Nguyen, L. T.; Chau, J. K.; Perry, N. A.; De Boer, L.; Zaat, S. A.; Vogel, H. J. Serum stabilities of short tryptophan-and arginine-rich antimicrobial peptide analogs. *PLoS One* **2010**, *5*, e12684−12691.
(36) Dathe, M.; Nikolenko, H.; Klose, J.; Bienert, M. Cyclization increases the antimicrobial activity and selectivity of arginine-and tryptophan-containing hexapeptides. *Biochemistry* **2004**, *43*, 9140−9150.
(37) Oh, D.; Sun, J.; Nasrolahi Shirazi, A.; LaPlante, K. L.; Rowley, D. C.; Parang, K. Antibacterial activities of amphiphilic cyclic cell-penetrating peptides against multidrug-resistant pathogens. *Mol. Pharmaceutics* **2014**, *11*, 3528−3536.
(38) Gunasekaran, P.; Kim, E. Y.; Lee, J.; Ryu, E. K.; Shin, S. Y.; Bang, J. K. Synthesis of Fmoc-Triazine amino acids and its application in the synthesis of short antibacterial peptidomimetics. *Int. J. Mol. Sci.* **2020**, *21*, 3602−3622.
(39) Lee, J.; Kang, D.; Choi, J.; Huang, W.; Wadman, M.; Barron, A. E.; Seo, J. Effect of side chain hydrophobicity and cationic charge on antimicrobial activity and cytotoxicity of helical peptoids. *Bioorg. Med. Chem. Lett.* **2018**, *28*, 170−173.
(40) Chongsiriwatana, N. P.; Patch, J. A.; Czyzewski, A. M.; Dohm, M. T.; Ivankin, A.; Gidalevitz, D.; Zuckermann, R. N.; Barron, A. E. Peptoids that mimic the structure, function, and mechanism of helical antimicrobial peptides. *Proc. Natl. Acad. Sci. U. S. A.* **2008**, *105*, 2794−2799.
(41) Padhee, S.; Hu, Y.; Niu, Y.; Bai, G.; Wu, H.; Costanza, F.; West, L.; Harrington, L.; Shaw, L. N.; Cao, C.; et al. Non-hemolytic α-AApeptides as antimicrobial peptidomimetics. *Chem. Commun.* **2011**, *47*, 9729−9731.
(42) Shi, Y.; Yin, G.; Yan, Z.; Sang, P.; Wang, M.; Brzozowski, R.; Eswara, P.; Wojtas, L.; Zheng, Y.; Li, X.; et al. Helical sulfono-γ-

AApeptides with aggregation-induced emission and circularly polarized luminescence. *J. Am. Chem. Soc.* **2019**, *141*, 12697−12706.
(43) Ting, D. S. J.; Beuerman, R. W.; Dua, H. S.; Lakshminarayanan, R.; Mohammed, I. Strategies in translating the therapeutic potentials of host defense peptides. *Front. Immunol* **2020**, *11*, 983−998.
(44) Imura, Y.; Nishida, M.; Ogawa, Y.; Takakura, Y.; Matsuzaki, K. Action mechanism of tachyplesin I and effects of PEGylation. *Biochim. Biophys. Acta, Biomembr.* **2007**, *1768*, 1160−1169.
(45) Singh, S.; Papareddy, P.; Morgelin, M.; Schmidtchen, A.; Malmsten, M. Effects of PEGylation on membrane and lipopolysaccharide interactions of host defense peptides. *Biomacromolecules* **2014**, *15*, 1337−1345.
(46) Albada, H. B.; Prochnow, P.; Bobersky, S.; Langklotz, S.; Schriek, P.; Bandow, J. E.; Metzler-Nolte, N. Tuning the activity of a short Arg-Trp antimicrobial peptide by lipidation of a C-or N-terminal lysine side-chain. *ACS Med. Chem. Lett.* **2012**, *3*, 980−984.
(47) Makovitzki, A.; Avrahami, D.; Shai, Y. Ultrashort antibacterial and antifungal lipopeptides. *Proc. Natl. Acad. Sci. U. S. A.* **2006**, *103*, 15997−16002.
(48) Tan, T.; Wu, D.; Li, W.; Zheng, X.; Li, W.; Shan, A. High specific selectivity and membrane-active mechanism of synthetic cationic hybrid antimicrobial peptides based on the peptide FV7. *Int. J. Mol. Sci.* **2017**, *18*, 339−355.
(49) Bagheri, M.; Hancock, R. E. High-performance liquid chromatography and mass spectrometry-based design of proteolytically stable antimicrobial peptides. *Antimicrobial Peptides. Methods in Molecular Biology*, Vol. *1548*; Hansen, P., Ed.; Humana Press: New York, 2017; pp 61−71. DOI: 10.1007/978-1-4939-6737-7_5.
(50) Bagheri, M.; Arasteh, S.; Haney, E. F.; Hancock, R. E. Tryptic stability of synthetic bactenecin derivatives is determined by the side chain length of cationic residues and the peptide conformation. *J. Med. Chem.* **2016**, *59*, 3079−3086.
(51) Karstad, R.; Isaksen, G.; Wynendaele, E.; Guttormsen, Y.; De Spiegeleer, B.; Brandsdal, B. O.; Svendsen, J. S.; Svenson, J. Targeting the S1 and S3 subsite of trypsin with unnatural cationic amino acids generates antimicrobial peptides with potential for oral administration. *J. Med. Chem.* **2012**, *55*, 6294−6305.
(52) Henklein, P.; Bruckdorfer, T. Shorter arginine homologues to stabilize peptides towards tryptic digestion. *Chim. Oggi (Chem. Today)* **2008**, *26*, 12−15.
(53) Chen, C.; Hu, J.; Zeng, P.; Chen, Y.; Xu, H.; Lu, J. R. High cell selectivity and low-level antibacterial resistance of designed amphiphilic peptide G (IIKK) 3I-NH2. *ACS Appl. Mater. Interfaces* **2014**, *6*, 16529−16536.
(54) Arias, M.; Piga, K. B.; Hyndman, M. E.; Vogel, H. J. Improving the activity of Trp-rich antimicrobial peptides by Arg/Lys substitutions and changing the length of cationic residues. *Biomolecules* **2018**, *8*, 19−35.
(55) Nguyen, L. T.; de Boer, L.; Zaat, S. A.; Vogel, H. J. Investigating the cationic side chains of the antimicrobial peptide tritrpticin: hydrogen bonding properties govern its membrane-disruptive activities. *Biochim. Biophys. Acta, Biomembr.* **2011**, *1808*, 2297−2303.
(56) Russell, A. L.; Williams, B. C.; Spuches, A.; Klapper, D.; Srouji, A. H.; Hicks, R. P. The effect of the length and flexibility of the side chain of basic amino acids on the binding of antimicrobial peptides to zwitterionic and anionic membrane model systems. *Bioorg. Med. Chem.* **2012**, *20*, 1723−1739.
(57) Lu, J.; Xu, H.; Xia, J.; Ma, J.; Xu, J.; Li, Y.; Feng, J. D- and unnatural amino acid substituted antimicrobial peptides with improved proteolytic resistance and their proteolytic degradation characteristics. *Front. Microbiol* **2020**, *11*, 563030.
(58) Pandit, G.; Ilyas, H.; Ghosh, S.; Bidkar, A. P.; Mohid, S. A.; Bhunia, A.; Satpati, P.; Chatterjee, S. Insights into the mechanism of antimicrobial activity of seven-residue peptides. *J. Med. Chem.* **2018**, *61*, 7614−7629.
(59) Aoki, W.; Ueda, M. Characterization of antimicrobial peptides toward the development of Novel Antibiotics. *Pharmaceuticals.* **2013**, *6*, 1055−81.
(60) Ghosh, S.; Pandit, G.; Debnath, S.; Chatterjee, S.; Satpati, P. Effect of monovalent salt concentration on the secondary structure in peptide-micelle binding. *RSC Adv.* **2021**, *11*, 36836−36849.
(61) Pandit, G.; Chowdhury, N.; Abdul Mohid, S.; Bidkar, A. P.; Bhunia, A.; Chatterjee, S. Effect of secondary structure and side chain length of hydrophobic amino acid residues on the antimicrobial activity and toxicity of 14-residue-long de novo AMPs. *ChemMedChem* **2021**, *16*, 355−367.
(62) Pandit, G.; Biswas, K.; Ghosh, S.; Debnath, S.; Bidkar, A. P.; Satpati, P.; Bhunia, A.; Chatterjee, S. Rationally designed antimicrobial peptides: Insight into the mechanism of eleven residue peptides against microbial infections. *Biochim. Biophys. Acta, Biomembr.* **2020**, *1862*, 183177−183192.
(63) Romoli, O.; Mukherjee, S.; Mohid, S. A.; Dutta, A.; Montali, A.; Franzolin, E.; Brady, D.; Zito, F.; Bergantino, E.; Rampazzo, C.; et al. Enhanced silkworm cecropin B antimicrobial activity against Pseudomonas aeruginosa from single amino acid variation. *ACS Infect. Dis.* **2019**, *5*, 1200−1213.
(64) Gaglione, R.; Cesaro, A.; Dell'Olmo, E.; Della Ventura, B.; Casillo, A.; Di Girolamo, R.; Velotta, R.; Notomista, E.; Veldhuizen, E. J.; Corsaro, M. M.; et al. Effects of human antimicrobial cryptides identified in apolipoprotein B depend on specific features of bacterial strains. *Sci. Rep.* **2019**, *9*, 6728.
(65) Halder, S.; Yadav, K. K.; Sarkar, R.; Mukherjee, S.; Saha, P.; Haldar, S.; Karmakar, S.; Sen, T. Alteration of zeta potential and membrane permeability in bacteria: a study with cationic agents. *SpringerPlus* **2015**, *4*, 672.
(66) Schrödinger, L. *The PyMOL Molecular Graphics System*, Version 2.0; Schrödinger, 2017.
(67) Gfeller, D.; Michielin, O.; Zoete, V. SwissSidechain: a molecular and structural database of non-natural sidechains. *Nucleic Acids Res.* **2012**, *41*, D327−D332.
(68) Cheng, X.; Jo, S.; Lee, H. S.; Klauda, J. B.; Im, W. CHARMM-GUI micelle builder for pure/mixed micelle and protein/micelle complex systems. *J. Chem. Inf. Model.* **2013**, *53*, 2171−2180.
(69) Mackerell, A. D., Jr Molecular dynamics simulation analysis of a sodium dodecyl sulfate micelle in aqueous solution: decreased fluidity of the micelle hydrocarbon interior. *J. Phys. Chem.* **1995**, *99*, 1846−1855.
(70) Rakitin, A. R.; Pack, G. R. Molecular dynamics simulations of ionic interactions with dodecyl sulfate micelles. *J. Phys. Chem. B* **2004**, *108*, 2712−2716.
(71) Wang, Q.; Hong, G.; Johnson, G. R.; Pachter, R.; Cheung, M. S. Biophysical properties of membrane-active peptides based on micelle modeling: a case study of cell-penetrating and antimicrobial peptides. *J. Phys. Chem. B* **2010**, *114*, 13726−13735.
(72) Lebecque, S.; Crowet, J. M.; Nasir, M. N.; Deleu, M.; Lins, L. Molecular dynamics study of micelles properties according to their size. *J. Mol. Graphics Modell.* **2017**, *72*, 6−15.
(73) Abraham, M.; van der Spoel, D.; Lindahl, E.; Hess, B.; G. Development Team. *GROMACS User Manual* 2019; https://www.gromacs.org
(74) Best, R. B.; Zhu, X.; Shim, J.; Lopes, P. E.; Mittal, J.; Feig, M.; MacKerell, A. D., Jr Optimization of the additive CHARMM all-atom protein force field targeting improved sampling of the backbone ϕ, ψ and side-chain χ1 and χ2 dihedral angles. *J. Chem. Theory Comput.* **2012**, *8*, 3257−3273.
(75) Durell, S. R.; Brooks, B. R.; Ben-Naim, A. Solvent-induced forces between two hydrophilic groups. *J. Phys. Chem.* **1994**, *98*, 2198−2202.
(76) Kabsch, W.; Sander, C. Dictionary of protein secondary structure: pattern recognition of hydrogen-bonded and geometrical features. *Biopolymers* **1983**, *22*, 2577−2637.
(77) Eisenhaber, F.; Lijnzaad, P.; Argos, P.; Sander, C.; Scharf, M. The double cubic lattice method: efficient approaches to numerical integration of surface area and volume and to dot surface contouring of molecular assemblies. *J. Comput. Chem.* **1995**, *16*, 273−284.
(78) Bondi, A. v. van der Waals volumes and radii. *J. Phys. Chem.* **1964**, *68*, 441−451.

https://doi.org/10.1021/acsomega.2c01089
ACS Omega 2022, 7, 15951−15968

(79) *Origin Pro*; OriginLab Corp.: Northampton, MA, USA, **2016**.

https://doi.org/10.1021/acsomega.2c01089
ACS Omega 2022, 7, 15951−15968